

A Review of Vessel Extraction Techniques and Algorithms

CEMIL KIRBAS

Wallace-Kettering Neuroscience Institute

AND

FRANCIS QUEK

Virginia Tech University

Abstract. Vessel segmentation algorithms are the critical components of circulatory blood vessel analysis systems. We present a survey of vessel extraction techniques and algorithms. We put the various vessel extraction approaches and techniques in perspective by means of a classification of the existing research. While we have mainly targeted the extraction of blood vessels, neurovascular structure in particular, we have also reviewed some of the segmentation methods for the tubular objects that show similar characteristics to vessels. We have divided vessel segmentation algorithms and techniques into six main categories: (1) pattern recognition techniques, (2) model-based approaches, (3) tracking-based approaches, (4) artificial intelligence-based approaches, (5) neural network-based approaches, and (6) tube-like object detection approaches. Some of these categories are further divided into subcategories. We have also created tables to compare the papers in each category against such criteria as dimensionality, input type, preprocessing, user interaction, and result type.

Categories and Subject Descriptors: A.1 [**General Literature**]: Introductory and Survey; I.2.10 [**Artificial Intelligence**]: Vision and Scene Understanding; I.4 [**Computing Methodologies**]: Image Processing and Computer Vision; I.5 [**Computing Methodologies**]: Pattern Recognition

General Terms: Algorithms, Design, Performance

Additional Key Words and Phrases: Magnetic resonance angiography, medical imaging, neurovascular, vessel extraction, X-ray angiography

1. INTRODUCTION

Blood vessel delineation on medical images forms an essential step in solving several practical applications such as diagnosis of the vessels (e.g., stenosis or malformations) and registration of patient images obtained at different times. Ves-

sel segmentation algorithms are the key components of automated radiological diagnostic systems. Segmentation methods vary depending on the imaging modality, application domain, method being automatic or semi-automatic, and other specific factors. There is no single segmentation method that can extract vasculature

Authors' addresses: C. Kirbas, Wallace-Kettering Neuroscience Institute, 3533 Southern Blvd., Suite 5200, Kettering, OH 45429; F. Quek, Center for Human-Computer Interaction, Virginia Tech University, 618 McBryde Hall, Blacksburg, VA 24061. Corresponding email: ckirbas@fastmail.fm.

Permission to make digital/hard copy of part or all of this work for personal or classroom use is granted without fee provided that the copies are not made or distributed for profit or commercial advantage, the copyright notice, the title of the publication, and its date appear, and notice is given that copying is by permission of ACM, Inc. To copy otherwise, to republish, to post on servers, or to redistribute to lists requires prior specific permission and/or a fee.

©2004 ACM 0360-0300/04/0600-0081 \$5.00

from every medical image modality. While some methods employ pure intensity-based pattern recognition techniques such as thresholding followed by connected component analysis [Higgins et al. 1989; Niki et al. 1993], some other methods apply explicit vessel models to extract the vessel contours [Molina et al. 1998; Klein et al. 1994, 1997]. Depending on the image quality and the general image artifacts such as noise, some segmentation methods may require image preprocessing prior to the segmentation algorithm [Guo and Richardson 1998; Sato et al. 1998b]. On the other hand, some methods apply post-processing to overcome the problems arising from over segmentation.

We survey current vessel segmentation methods, covering both early and recent literature related to vessel segmentation algorithms and techniques. Application domain of these techniques includes; (i) extraction of neurovascular structures, (ii) retinal blood vessel segmentation, (iii) coronary artery extraction, (iv) extraction of blood vessels from mammograms, (v) human airway tree (pulmonary tree) segmentation, (vi) extraction of abdominal aorta and vascular structures in the legs, (vii) extraction of vascular structures in livers, (viii) colon extraction, (ix) segmentation of nerve channels, and (x) extraction of tubular structures for industrial and scientific applications.

We introduce each segmentation method category and briefly summarize papers by category. We aim to give a quick summary of the papers and refer interested readers to references for additional information. At the end of each section, we provide a table and compare the methods reviewed in that section. The comparison includes segmentation method category, input image type such as XRA, MRA, MRI, CT, etc., dimensionality, use of a priori knowledge, whether the method employs multi-scale technique, user interaction requirement, result type such as centerline, vessel edges, and junctions, and whether the method segments the whole vessels tree or not.

Interested readers are referred to several surveys on medical image segmentation and analysis in general [McInerney and Terzopoulos 1996; Chen et al. 1999; Ayache 1994; Duncan and Ayache 2000; Clarke et al. 1995], and vessel visualization and quantification in particular [Felkel et al. 2001; Buhler et al. 2002] for further reading.

This article is organized as follows: In Section 2, the classification of the extraction methods is given. In Section 3, pattern recognition techniques are reviewed. Model-based approaches are discussed in Section 4. In Section 5, tracking-based approaches are reviewed. Methods based on artificial intelligence are discussed in Section 6. In Section 7, neural network-based methods are reviewed. In Section 8, algorithms that are not particularly designed to extract vessels but deal with extraction of tubular objects are discussed. We conclude with discussion on the issues related to vessel extraction and its applications in Section 9.

2. CLASSIFICATION OF VESSEL EXTRACTION TECHNIQUES AND ALGORITHMS

We did not enforce any taxonomy at the beginning of writing this survey. Instead, we put papers that use similar approaches into same group while we review them. During the categorization, we tried to be as specific as possible. For this reason we divided some categories into subcategories as necessary. We also created a separate category for some methods that are used significantly. For example, we created a separate category for *generalized cylinders model* approach even it is a *parametric model* because of the amount of work done using this model.

I. Pattern recognition techniques

- A.** Multi-scale approaches
- B.** Skeleton-based approaches
- C.** Region growing approaches
- D.** Ridge-based approaches
- E.** Differential geometry-based approaches

- F.** Matching filters approaches
- G.** Mathematical morphology schemes
- II.** Model-based approaches
 - A.** Deformable models
 - a.** Parametric deformable models—Active contours (Snakes)
 - b.** Geometric deformable models and front propagation methods
 - c.** Deformable template matching approaches
 - B.** Parametric models
 - C.** Generalized cylinders approaches
- III.** Tracking-based approaches
- IV.** Artificial Intelligence-based approaches
- V.** Neural Network-based approaches
- VI.** Tube-like object detection approaches

Although we divide segmentation methods in different categories, sometimes multiple techniques are used together to solve different segmentation problems. We, therefore, cross-listed the methods that fall into multiple segmentation categories. Such methods are reviewed in one section and mentioned in the other section with a pointer referencing to the section in which it is reviewed.

3. PATTERN RECOGNITION TECHNIQUES

Pattern recognition (PR) techniques deal with the automatic detection or classification of objects or features. Humans are very well adapted to carry out PR tasks. Some of the PR techniques are the adaptation of human PR ability to the computer systems. In the vessel extraction domain, PR techniques are concerned with the detection of vessel structures and the vessel features automatically. We divide PR techniques into seven categories: (1) multiscale approaches, (2) skeleton-based (centerline detection) approaches, (3) region growing approaches, (4) ridge-based approaches, (5) differential Geometry-based approaches, (6) matching filters approaches, and (7) mathematical morphology schemes. In the next sections, each

category is discussed and the literature related to each category is reviewed.

3.1. Multi-scale Approaches

Multi-scale approaches perform segmentation at varying image resolutions. The main advantage of this technique is increased processing speed. Major structures (large vessels in our application domain) are extracted from low resolution images while fine structures are extracted at high resolution. Another advantage is increased robustness. After segmenting the strong structures at the low resolution, weak structures, such as branches, in the neighborhood of the strong structures can be segmented at higher resolution.

Sarwal and Dhawan [1994] reconstruct 3D coronary arteries from three views by matching branch points in each view. Their method is based on simplex method-based linear programming and relaxation-based consistent labeling. To improve the robustness of the matcher, matching process is performed at three different resolutions. The stronger vessel tree branches are extracted at lower resolution while the weaker branches are extracted at higher scale. The extracted vessel tree is used for 3D reconstruction.

Chwialkowski et al. [1996] employ multiresolution analysis based on wavelet transform. Their work aims at automated qualitative analysis of arterial flow using velocity-sensitive, phase contrast MR images. The segmentation process is applied to the magnitude image and the velocity information from the phase difference image is integrated on the resulting vessel area to get the blood flow measurement. Vessel boundaries are localized by employing a multivariate scoring criterion to minimize the effect of imaging artifacts such as partial volume averaging and flow turbulence. This method can also be classified as a contour detection approach.

The works of Summers and Bhalerao [1995] described in Section 4.1.3, Huang and Stockman [1993] described in Section 8, and Armande et al. [1999] described in Section 3.3 employ a multiscale

approach and can also be listed in this section.

3.2. Skeleton-Based (Centerline Detection) Approaches

Skeleton-based methods extract blood vessel centerlines. The vessel tree is created by connecting these centerlines. Different approaches are used to extract the centerline structure. Some of these methods are: (i) apply thresholding and then object connectivity, (ii) thresholding followed by a thinning procedure, and (iii) extraction based on graph description. The resulting centerline structure is used for 3D reconstruction.

Niki et al. [1993] describe a 3D blood vessel reconstruction and analysis method. Vessel reconstruction is achieved on short scan cone-beam filtered back-propagation reconstruction algorithm based on Gulberg and Zeng's work [Gullberg and Zeng 1992]. A 3D thresholding and 3D object connectivity procedure are applied to the resulting reconstructed images for the visualization and analysis process. A 3D graph description of blood vessels is used to represent the vessel anatomical structure.

Tozaki et al. [1995] extract bronchus and blood vessels from thin slice CT images of the lung for 3D visualization and analysis. First, a threshold is used to segment the images. Then, blood vessels and bronchus are differentiated by using their anatomical character (e.g., the bronchus contain air). Finally, a 3D thinning algorithm is applied to extract the vessel centerlines. The resulting centerline structure is used to analyze and classify the blood vessels. Their work helps in early detection of tumors of lung cancer patients.

Kawata et al. [1995a] analyze blood vessel structures and detect blood vessel diseases from cone-beam CT images. X-ray digital angiograms are collected using rotational angiography. 3D image reconstruction is performed by a short scan cone-beam filtered backprojection algorithm based on the short injection time of the contrast medium. First, a graph description procedure extracts the curvi-

linear centerline structures of the vessel tree using thresholding, elimination of the small connected components, and 3D fusion processes. Then, a 3D surface representation procedure extracts the characteristics of convex and concave shapes on blood vessel surface. The algorithm is run on a set of patient images with abdominal blood vessels, with two aneurysms and one stenosis, and the results are shown.

Kawata et al. [1995b] detect blood vessel diseases on high resolution 3D cone-beam CT images. This method has two major components: (1) A graph description procedure extracts a graph description of vessel centerlines from the vessel image; (2) A surface representation procedure extracts concave and convex shapes on vessels using curvature. These shapes are used to represent aneurysms and stenoses on the vessels. Vessel surfaces are represented by curvatures which are invariant to arbitrary translations and rotations. Surface characteristics such as Gaussian (K) and mean (H) curvatures, principal directions, surface normal direction, curvature magnitude, and surface types using signs of K and H can be obtained easily from the surface representation using curvatures. Since blood vessels' surfaces are represented using curvatures, this work can also be classified as a *differential geometry-based approach* listed in Section 3.5.

Parker et al. [1988] gives a theoretical review of 3D reconstruction algorithm of vascular networks from X-ray projection images. The algorithm has two steps: (1) Segmenting the centerline positions and densimetric profiles of artery candidates from each projection image; and (2) Combining multiple view information gathered in step one into one 3D artery representation in an iterative fashion. Their work utilizes intrinsic vascular bed properties such as connectivity, density, and lumen dimensions in the reconstruction process.

Sorantin et al. [2002] uses a 3D skeletonization method in the assessment of tracheal stenoses on spiral CT images. The method consists of five steps: (1) Laryngotracheal tract (LTT) is segmented using

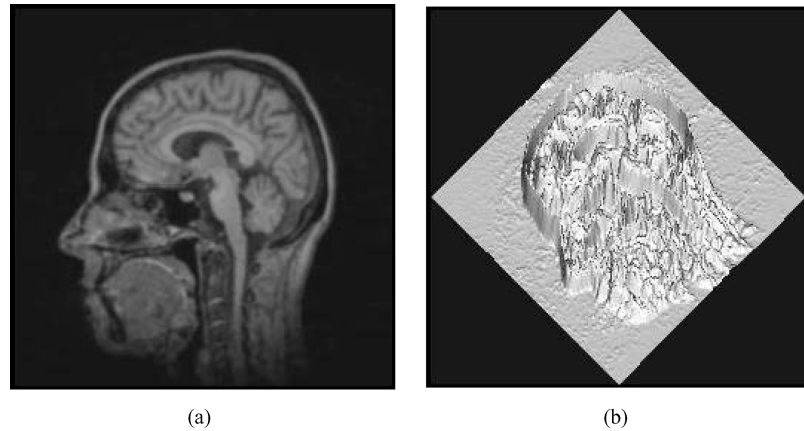


Fig. 1. (a) An MRI slice, and (b) Associated 2D intensity map in 3D (Reproduced from Aylward et al. [1996]).

fuzzy connectedness. The system extracts LTT as a single object starting from a user-supplied *seed point*. A 3D dilation is employed to handle the uncertain boundary points due to partial volume effect. The segmented binary 3D volume is, then, converted into cubic voxels by linear interpolation; (2) 3D thinning operation is applied to the resulting 3D volume; (3) LLT medial axis is separated from the extracted skeleton using a shortest path-searching algorithm. This step requires the user to mark begin end end points on the central path; (4) Segmented LTT medial axis, represented by a sequence of vectors, is smoothed; and (5) LTT cross-sectional profile along the medial axis is calculated. The technique is reported as “highly accurate and precise” based on the phantom studies.

The works of Poli and Valli [1997] reviewed in Section 3.6, Mao et al. [1992] reviewed in Section 3.6, Prinet et al. [1996, 1997], reviewed in Section 3.5, Eiho and Qian [1997] and Haris et al. [1997a] reviewed in Section 3.7, O’Brien and Ezquerra [1994] reviewed in Section 3.4, Yim et al. [2000] reviewed in Section 3.4, Higgins et al. [1989] reviewed in Section 3.4, and Armande et al. [1999] described in Section 3.3 can also be classified as a *skeleton-based* approach due to the skeleton detection in the segmentation process.

3.3. Ridge-Based Approaches

Ridge-based methods treat grayscale images as 3D elevation maps in which intensity ridges approximate the skeleton of the tubular objects [Aylward et al. 1996]. Figure 1 shows a MRI slice and its corresponding 2D intensity height surface in 3D. After creating the intensity map, ridge points are local peaks in the direction of maximal surface gradient, and can be obtained by tracing the intensity map from an arbitrary point, along the steepest ascent direction. Ridges are invariant to affine transformations and can be detected in different image modalities. These properties are exploited in medical image registration [Aylward et al. 1996, 2002; Aylward and Bullitt 2001]. Since ridge-based approaches detect skeleton of tubular objects, it can be thought of as a specialized skeleton-based approaches.

Bullitt and Aylward [2001] describe their method of defining *vessel trees* from 3D image volume. The segmentation stage starts with a manually-selected seed point for each vessel. The system extracts an intensity ridge map which represents the vessel’s medial axis. Vessel width at each ridge point is also calculated using a scale-based approach. The vessel tree is represented by a graph where each vessel keeps information about its relationship to other

vessels. Some other publications of the authors describe the issues related to segmentation and graph description in detail [Aylward et al. 1996; Bullitt et al. 1999, 2001; Aylward and Bullitt 2002]. The main application of this work is the registration of vasculature images obtained from the same patient at different times. This allows the observation of changes in pathology over time.

Guo and Richardson [1998] propose a ridge extraction method that treats digitized angiograms as height maps and the centerlines of the vessels as ridges in the map. The image is first balanced by a median filter and then smoothed by a nonlinear diffusion method (anisotropic smoothing). Then, a region of interest is selected by adaptive thresholding method. This process cuts the cost of the ridge extraction process and reduces false ridges introduced by noise. Next, the ridge detection process is applied to extract the vessel centerlines. Finally, the candidate vessel centerlines are connected using a curve relaxation process.

Aylward et al. [1996] approximate the medial axes of tubular objects such as vessels in an angiogram as directed “intensity ridges”. They apply the *cores* method [Pizer et al. 1998] which has been proven to be invariant to a wide range of noise and object disturbances. Ridges are tracked by estimating the local vessel directions. First, image intensity is mapped to height to create intensity height surface. Second, from a user-supplied starting point an initial ridge point is found using a conjugate directions search with respect to the Hessian matrix. Third, the ridge is tracked. Finally, the local widths of the segmented object is estimated using points on the ridges. The authors show results of a vascular tree extracted from a MR angiogram. This required a fair amount of user intervention (105 mouse clicks in all). Figure 2 shows the extracted vascular tree.

The work of Chandrinos et al. [1998] described in Section 5 can also be classified as a *ridge-based* approach due to the ridge detection in the segmentation process.

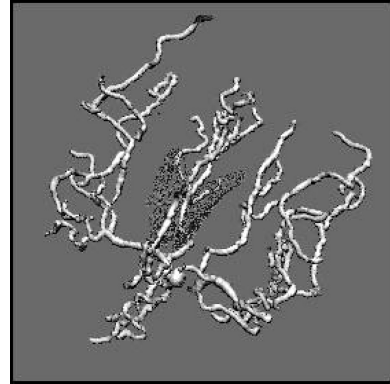


Fig. 2. Vessel tree extracted from 105 mouse clicks (Reproduced from Aylward et al. [1996]).

3.4. Region Growing Approaches

Starting from some seed point, region growing techniques segment images by incrementally recruiting pixels to a region based on some predefined criteria. Two important segmentation criteria are *value similarity* and *spatial proximity* [Jain et al. 1995]. It is assumed that pixels that are close to each other and have similar intensity values are likely to belong to the same object. The main disadvantage of region growing approach is that it often requires user-supplied seed points. Due to the variations in image intensities and noise, region growing can result in holes and over-segmentation. Thus, it requires post-processing of the segmentation result.

Schmitt et al. [2002] determine contrast agent propagation in 3D rotational XRA image volumes. They combine thresholding with a region growing technique to segment vessel tree in 3D. The optimal threshold is determined experimentally. After the segmentation, propagation information is mapped from the 2D projections to the 3D image data set created by the rotational XRA.

O'Brien and Ezquerra [1994] automatically segment coronary vessels in angiograms based on temporal, spatial, and structural constraints. The algorithm starts with a low pass filtering applied to the image as preprocessing. Then, initial segmentation starts with a user-supplied

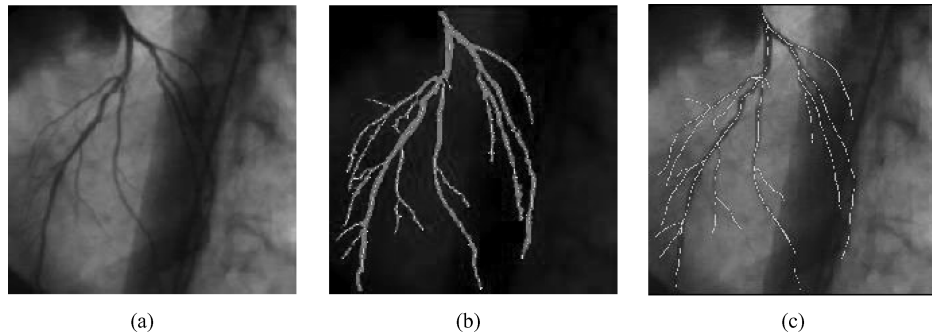


Fig. 3. (a) The original XRA image, (b) Initial segmentation and expansion results, and (c) The final result (Reproduced from O'Brien and Ezquerre [1994]).

seed point. The system starts a region growing process to extract the initial approximation to the vessel structure. After that, the centerlines are extracted by employing a *balloon test*. Next, undetected vessel segments are located by a spatial expansion algorithm. At this stage, images are divided into two categories: vessel areas and nonvessel areas. However, there is no spatial or temporal connectivity information exists in the detected sub-regions. This information is extracted by applying an acceptance and rejection test using graph theory. Figure 3 shows the result of their method applied to an angiogram image. Due to the extraction of the centerlines, this work can also be classified as a *skeleton-based* approach listed in Section 3.2.

Higgins et al. [1989] describe their automatic arterial tree extraction algorithm from 3D coronary angiograms. These angiograms are obtained from high-resolution X-ray CT scanner known as 3D Dynamic Spatial Reconstructor (DSR). Their algorithm is a combination of a 3D filter, a connected component analysis, a thresholding process, and seeded region growing algorithm. The strength of the algorithm is reported as the results being reproducible, requiring less user time, and working in 3D. Due to the skeleton detection process performed, this work can also be classified as a SBA listed in Section 3.2.

Yim et al. [2000] determine vessel tree structures from MRA images using a gray-scale skeletonizing method based on

the ordered region-growing algorithm that represents the image as an acyclic graph using the image voxels connectivity. A distinctive feature of this method is that the path used in the graph has minimal dependence on seed location that makes the method reliable on every part of the graph, not only in the vicinity of the seed point. After forming the acyclic graph, a skeletonizing process is applied to extract the tree in two different methods. In the first method, user explicitly selects the origin, which serves as the seed point of the graph, of the tree and endpoints of the vessels. Then, vessel segments are extracted by tracing the path from each endpoint to the origin of the graph. The second method uses a pruning process based on the branch length. It requires a user-supplied seed point and two parameters that describe the desired topology of the tree. The method retains vessel segments which have the length more than the specified length and discards the others. The ordered region growing method resolves the ambiguities in the tree branching due to vessel overlap by incorporating *a priori* knowledge about the bifurcation spacing. Due to the skeletonization process applied to extract tree, this work can also be classified as a *skeleton-based* approach listed in Section 3.2.

Higgins et al. [1996] develop a system to extract, analyze, and visualize coronary arteries from high-resolution 3D angiograms using *Artery Extractor*, *Tree Trace*, and *Artery Display* tools created.

The steps in arterial tree extraction are as follows: (1) A 3D image filter is applied to reduce the noise and artifact effects; (2) A thresholding operation is performed to isolate large and very bright regions which form the seed regions of the tree; (3) An iterative 3D seeded region growing algorithm is employed to build up the tree from the seed regions; and (4) A cavity filling process is applied to add the cavities missed during seeded region growing process. After the tree is extracted, an axes generation process is employed to get the skeleton as follows: (1) The large aortic root is removed to leave the tree branches; (2) 3D skeleton of all branches is computed using an iterative skeletonization process that uses 26-connectivity; (3) The skeletal components of useless short branches are pruned; and (4) Remaining skeletal components are combined into line segments.

The work of Donizelli [1998] reviewed in Section 3.7 can be classified as a *region growing approach* due to the binary region growing algorithm applied.

3.5. Differential Geometry-Based Approaches

Differential geometry (DG)-based methods treat images as hypersurfaces and extracts features using the curvature and the crest lines of the surface. The crest points of the hyper-surface correspond to the center lines of the vessel structure. The 2D and 3D images are treated similarly, being modelled as 3D and 4D hypersurfaces respectively. In DG, a 3D surface can be described by two principal curvatures and by their corresponding orthogonal directions, called principal directions. These features are also invariant under affine transformations and therefore well-suited to medical image registration [Guéziec et al. 1997; Guéziec and Ayache 1994; Ayache et al. 1993]. The principal curvatures correspond to the eigenvalues of the Weingarten matrix and the principal directions are the eigenvectors. Crest points, which are the intrinsic properties of the surfaces, are the local maxima of the maximum curvature on the hypersurface. Crest lines are intuitively

the most salient features of the surfaces. Centerlines are obtained by linking the crest-points.

A good introduction to differential geometry can be found in Do Carmo [1976] and Koenderink [1990].

Krissian et al. [1996] describe their Directional Anisotropic Diffusion (DAD) method derived from Gaussian convolution to reduce the image noise. Their method, a more general form of work by Perona and Malik [1990], is based on the differentiation of the diffusion in the direction of the gradient, minimum, and maximum curvatures. DAD reduces the noise in the image without introducing blurring. The algorithm is applied to a set of phantom images containing torus with different radii and a set of vessel images. A comparison of the results of the anisotropic diffusion and Gaussian convolution method is given.

Prinet et al. [1997] propose a multidimensional vessel extraction method that treats images as parametric surfaces and extracts features of the images using surface curvature and the crest lines. When linked together, the crest points form the center lines of the vessels. Results of the algorithm applied to angiograms, 2D Digital Subtraction Angiography (DSA), Magnetic Resonance Angiography (MRA), and 3D synthetic data are reported. Due to the centerline detection performed, this work can also be classified as a *skeleton-based* approach listed in Section 3.2.

Prinet et al. [1996] describe the framework of their thin network extraction algorithm from volumetric images. The method uses differential geometry of the surfaces and treats 3D image volume as a hyper surface of 4D. The fact that the crest points of the hyper-surface correspond to the center line of the thin network in the volume image is utilized in the technique. A cylindrical mathematical model is used to represent the vessels. Vessel network is extracted by detecting the extrema of the maximal curvatures, that is, the crest points. The technique requires no a priori knowledge on the shape of the network and is entirely automatic. Due to the centerline detection performed, this work can

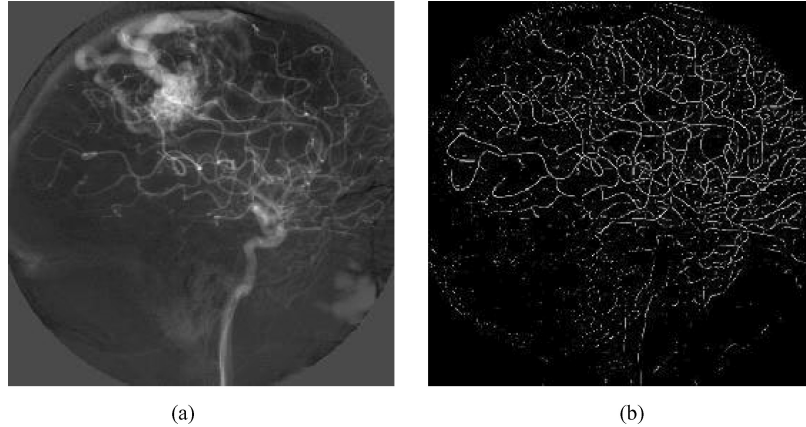


Fig. 4. (a) DSA image of the cerebral vessels, and (b) Vessel detection using four values of the scale (Reproduced from Armande et al. [1999]).

also be classified as a *skeleton-based approach* listed in Section 3.2.

Armande et al. [1999] extract thin nets using a MSA that exploits the DG properties of the image surface. They characterize thin nets as crest lines of the image surface. To overcome the problem faced in extraction of the thin nets having different widths, they employ a MSA. Their method consists of three main stages: (1) They detect the extrema of the maximum curvature for all scales; (2) They remove false responses, using the gradient zero-crossings; and (3) They select those points verified by medium scale expression as crest points. In some other works, they used similar approach in different application domains [Monga et al. 1994a, 1994b, 1997; Armande et al. 1995]. Figure 4 shows a DSA image and the extracted vessel network using four different scales. This work can also be classified as a MSA listed in Section 3.1.

The work of Zana and Klein [1997] described in Section 3.7 can be classified as a *differential geometry-based approach* due to the curvature differentiation procedure applied in the final step to extract the vessels.

The work of Kawata et al. [1995b] described in Section 3.2 can be classified as a *differential geometry-based approach* due to the representation of the blood vessels' surfaces using curvatures.

3.6. Matching Filters Approaches

Matching filters approach convolves the image with multiple matched filters for the extraction of objects of interest. In extracting vessel contours, designing different filters to detect the vessels with different orientation and size plays a crucial role. The convolution kernel size affects the computational load. Matching filters are usually followed with some other image processing operations like thresholding and connected component analysis to get the final vessel contours. Connected component analysis is preceded by a thinning process to detect vessel centerlines.

Sato et al. [1998b] introduce a 3D multiscale line enhancement filter to segment curvilinear structures in medical images. The filter is based on the directional second derivatives of smoothed images using Gaussian kernel in multiscales with adaptive orientation selection using the Hessian matrix. They demonstrate the result of their method applied to segment brain vessels from MRI/MRA and bronchi from a chest CT, and liver vessels from an abdominal CT. Figure 5 shows original and line filtered MR images. Figure 6 shows the volume rendered images of these images.

Poli and Valli [1997] develop an algorithm, based on a set of multiple oriented

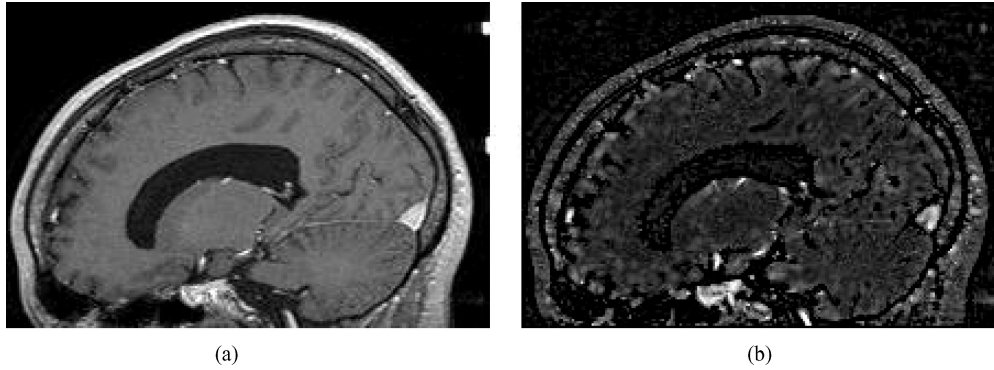


Fig. 5. (a) Original, and (b) Line filtered MR images (Reproduced from Sato et al. [1998a]).

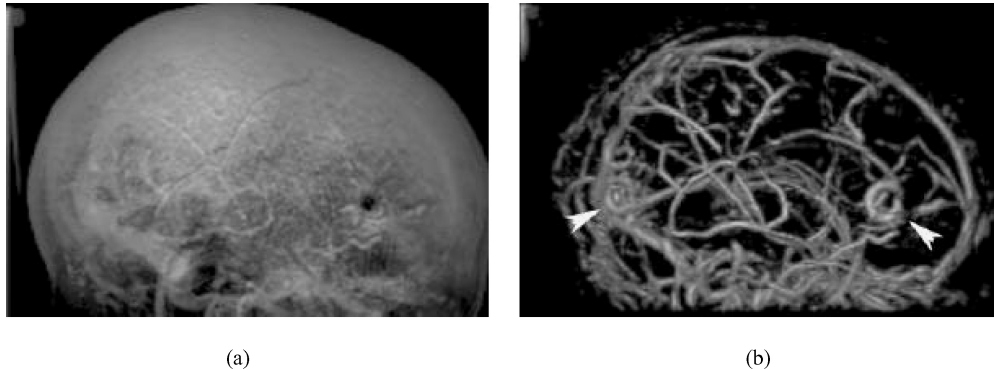


Fig. 6. Volume rendered (a) Original, and (b) Line filtered MR images (Reproduced from Sato et al. [1998a]).

linear filters obtained as linear combination of properly shifted Gaussian kernels, to enhance and detect vessels in real time. These filters are sensitive to vessels of different orientation and thickness. There are two distinctive features that make their algorithm different than other matched-filters-based algorithms: (1) Convolution masks are designed carefully to obtain maximum efficiency and (2) Output of the operators of different orientation and scale is integrated and validated to prevent the enhancement of the structures other than vessels. Vessel segmentation is achieved by employing a thresholding method called *thresholding with hysteresis* [Canny 1983]. The algorithm is run on synthetic and real coronary angiograms and the results are reported as promising. Due to the skeleton detection process performed, this work can also

be classified as a *skeleton-based* approach listed in Section 3.2.

Hart et al. [1997] describe an automated tortuosity measurement technique for blood vessel segments in retinal images. They use a filter developed by Chaudhuri et al. [1989] in the vessel extraction process. The filter is applied to the green plane of the RGB image since it typically exhibits the greatest contrast. The filter is applied at 12 orientations over 180 degree and the maximum response of these filters at each location is selected as the vessel edge. Then, a thresholding and thinning processes applied to get the binary image containing the vessel segments. The final set of vessel segments is obtained by applying a linear classifier algorithm, described in Cote et al. [1994]. A classification rate of 91% of blood vessel segments and 95% of vessel network is reported.

Wood et al. [1995] equalizes image variabilities as a preprocessing step in their method to segment retinal vessels. Image equalization is achieved by computing a local two dimensional average and subtracting from each pixel. This procedure normalizes the variation in the background level before edge detection. Then, a non-linear morphological filtering method is used to locate the vessel segments. The method is demonstrated on two images of the same patient taken at different times. Two images are thresholded resulting in two binary images from which the vessel structures are extracted. The resulting coordinate system is used to register the images and to remove the interference from the vessel structure for the analysis of the underlying retinal nerve fiber layer (RNFL).

Mao et al. [1992] describe their algorithm to extract structural features in digital subtraction angiograms. The algorithm is based on the visual perception modeling which states that the relevant parts of objects in noisy scenes are usually grouped together. A saliency map is constructed by grouping salient structures or curves iteratively. Centerlines and contours obtained from the structural feature extraction algorithm are, then, used to refine the extraction process. The problem with this algorithm is that it does not successfully solve all the 2D ambiguities such as crossing or forking situations. This method is aimed to detect the vascular structures from two X-ray projections for 3D reconstruction of vascular network. Due to the centerline detection performed, this work can also be classified as a *skeleton-based* approach listed in Section 3.2.

Hoover et al. [2000] combine local and region-based properties to segment blood vessels in retinal images. The method examines the matched filter response (MFR) [Chaudhuri et al. 1989], using a probing technique. The technique classifies pixels in an area of the MFR as vessels and nonvessels by iteratively decreasing the threshold. At each iteration, the probe examines the region-based attributes of the pixels in the tested area and segments

the pixels classified as vessels. Pixels that are not classified as vessel from probes are recycled for further probing. A unique feature of this method is that each pixel is classified using local and region-based properties. The method is evaluated using hand-labeled images and tested against basic thresholding of MFR. As much as 15 times reduction of false positives over the basic MFR and up to 75% true positive rate has been reported.

Chen et al. [1998, 2000] develop a method to segment lines, especially intersections (X-junctions) and branches (T-junctions), in multiple orientation using *orientation space filtering* technique. The unique feature of this method is that image is represented by what is called *orientation space* by adding orientation axis to the abscissa and the ordinate of the image. The orientation space representation is then treated as continuous variable to which Gabor filters, which represent lines at multiple orientations, can be tuned. Multiple orientation line detection is achieved by thresholding 3D image of the orientation space and then detecting the connected components in the resulting image. Selecting suitable bandwidth for the Gabor filter is an important issue that effects the sensitivity of the filters to the lines. If the orientation bandwidth is small, the orientation selectivity is high. On the other hand, the response of a line having a high degree of curvature is small which means the sensitivity of the line is low. This feature requires a trade-off between sensitivity and selectivity for optimum multiple orientation line segmentation. The method is tested on synthesized and real biomedical images and the results are discussed.

The work of Goldbaum et al. [1996] reviewed in Section 3.6 can be classified as a *matching filters* approach due to the rotated matched filters used in the segmentation process.

The work of Thirion et al. [2000] reviewed in Section 8 can be classified as a *matching filters* approach due to the bank of filters used in the segmentation process.

The work of Huang and Stockman [1993] reviewed in Section 8 can be

classified as a *matching filters* approach due to the optimal filters used in the segmentation process.

The works of Klein et al. [1994, 1997] reviewed in Section 4.1.1 can be classified as a *matching filters* approach due to the bank of orientation specific S-Gabor filter pairs used.

3.7. Mathematical Morphology Schemes

Morphology relates to the study of object forms or shapes. Morphological operators (MO) apply structuring elements (SE) to images, and are typically applied to binary images but can be extended to the gray-level images. *Dilation* and *erosion* are the two main MO. *Dilation* expands objects by a SE, filling holes, and connecting disjoint regions. *Erosion* shrinks objects by a SE. *Closing*, dilation followed by erosion, and *opening*, erosion followed by dilation, are two other operations. Two algorithms used in medical image segmentation and related to mathematical morphology are *top hat* and *watershed* transformations [Sonka and Hlavac 1999].

A good introduction to morphological operators can be found in Umbaugh [1998] and Jain et al. [1995].

Figueiredo and Leitao [1995] describe their nonsmoothing approach in estimating vessel contours in angiograms. Their technique has two key features: (1) It does not smooth the image to avoid the distortions introduced by smoothing; and (2) It does not assume a constant background which makes the technique well suited for the unsubtracted angiograms. Edge detection is achieved by adapting a morphological (nonlinear) gray scale edge operator. Linear operators, such as matched filters or derivative-based schemes, would not work under the assumptions mentioned above. All local maxima, for each vessel cross section, of the morphological edge detector are considered as candidate edge points. Then dynamic programming is used to find the minimum cost path among the candidates by selecting a pair for each cross-section. Continuity and intensity terms are used as adapted costs

in the process of selecting candidate edge points.

Haris et al. [1997a] combined a recursive sequential tracking algorithm and morphological tools of homotopy modification and watersheds to automatically extract coronary arteries from angiogram images. Initial segmentation of artery tree skeleton is achieved through a tracking method based on circular template analysis. The result of this process is an approximation of artery tree skeleton along with estimates of the artery width at each point. Then, the morphological tools of homotopy modification and watershed transform are used to analyze each artery segment for the accurate border extraction. Authors of the article admit that the system has problem in extracting complete coronary tree. Due to the skeletonization of artery tree, this work can also be classified as a *skeleton-based* approach listed in Section 3.2.

Eiho and Qian [1997] propose a method based on pure MO to detect coronary artery tree in cine-angiograms. The steps of the method are: (1) A *top-hat operator* is applied to enhance the shape of the vessels; (2) Morphological erosion followed by half-thresholding operations are applied to remove the areas that are not the coronary artery; (3) Starting from a user-supplied point on the tree, the system extracts whole tree using neighbor checking according to the average gray levels; (4) The extracted artery tree is skeletonized by the thinning operation; (5) The edges are extracted by applying *watershed transformation* on the binary image obtained from a dilation operation on the binary skeleton. Due to the skeletonization of artery tree, this work can also be classified as a *skeleton-based* approach listed in Section 3.2.

Donizelli [1998] combines mathematical morphology and region growing algorithms to segment large vessels from DSA images. First, mathematical "top-hat" algorithm, which is a morphological filter to extract line-like structures, is applied to extract large vessels. Then, a binary region growing algorithm is applied to get rid of some residual shorter capillaries

and background noise artifacts. Finally, a threshold is applied to eliminate small regions and to obtain the regions of the large vessels. The author implemented three other classical and morphological algorithms, multiphase analysis process (MRAP) [Stansfield 1986], region splitting approach (RSBA) [Kottke and Sun 1990a], and morphological-thresholding (ROSE) [Thackray and Nelson 1993], and compared with his method. Due to the binary region growing algorithm employed, this work can also be classified as a *region growing approach* listed in Section 3.4.

Zana and Klein [1997] present a vessel segmentation algorithm from retinal angiography images based on mathematical morphology and linear processing. A unique feature of the algorithm is that it uses a geometric model of all possible undesirable patterns that could be confused with vessels in order to separate vessels from them. As a first step, all bright round peaks are extracted that allows microaneurisms to be segmented from the angiograms of diabetic patients. The strength of the algorithm comes from the combination of mathematical morphology and differential operators in the segmentation process. Linear bright shapes and basic features are extracted using mathematical morphology operators and differential shape properties like curvature are computed using a Laplacian filter. Vessels are extracted using curvature differentiation in the final step. This work can also be classified as a *differential geometry-based approach* listed in Section 3.5.

Thackray and Nelson [1993] describe an approach which extracts vascular segments using a set of 8 morphological operators, each of which represents an oriented vessel segment. The system also applies an adaptive thresholding scheme to extract the vascular segments from the intensity image. The system was used to extract vessel segments in a capillary angiogram of mice, and does not extract the vascular interconnection structure. The range of vessel widths the system handles appears limited by the setting of the 8 morphological operators.

3.8. 3D Reconstruction of Vessels

The works of Sarwal and Dhawan [1994] in Section 3.1, Niki et al. [1993] in Section 3.2, Kawata et al. [1995a] in Section 3.2, Kawata et al. [1995b] in Section 3.2, and Parker et al. [1988] in Section 3.2 are related to 3D reconstruction of the vessels. A comparison table of papers reviewed in this section is given in Figure 7.

4. MODEL-BASED APPROACHES

Model-based approaches apply explicit vessel models to extract the vasculature. We divide model-based approaches into four categories: (1) Deformable models, (2) Parametric models, (3) Template matching, and (4) Generalized cylinders.

4.1. Deformable Models

We divide deformable models into two categories: parametric deformable models and geometric deformable models. These categories are discussed in detail in the next sections.

A survey on Deformable Models in medical image analysis is published by McInerney and Terzopoulos [1996]. Xu et al. [2000] published a book chapter on medical image segmentation using deformable models and another book chapter on current methods in medical image segmentation [Pham et al. 2000] which includes a section on deformable models.

4.1.1. Parametric Deformable Models—Active Contours (Snakes). Deformable models are model-based techniques that find object contours using parametric curves that deform under the influence of internal and external forces. First introduced by Kass, Witkin, and Terzopoulos in 1987 [Kass et al. 1988], active contour models or *snakes* are a special case of a more general technique of matching a deformable model by means of energy minimization. Physically, a snake is a set of control points, called *snaxels*, in an image that are connected to each other. Each snaxel has an associated energy that either rises or falls depending upon the forces that act on it. These forces are known as snake's

Algorithm	Year	Classification	Input Type	Dimension	Preprocessing	A priori Knowledge	Multi-scale Technique	User Interaction	Result Type			Whole Tree	
									2D	3D	Centerline		
MULTI-SCALE APPROACHES													
Sarwal and Dhawan[SarD94]	1994	MSA & 3D Recons	Coronary XRA	Yes	No	No	Yes	Yes	No	Yes	No	Yes	Yes
Chwialkowski et al[Chwetal96]	1996	MSA	Phase Contrast MRI	Yes	No	No	Yes	Yes	No	No	Yes	N/A	N/A
SKELETON-BASED APPROACHES													
Niki et al[Niketal93]	1993	SBA & 3D Rec.	Rotational XRA	No	Yes	Yes	Yes	No	No	Yes	No	Yes	Yes
Tozaki et al[Tozetal95]	1995	SBA & 3D Vis.	CT	No	Yes	No	Yes	No	N/A	Yes	No	Yes	Yes
Kawata et al[Kawetal95a]	1995	SBA & DGBA	Cone-beam CT	No	Yes	No	Yes	No	N/A	Yes	No	Yes	Yes
Kawata et al[Kawetal95b]	1995	SBA & DGBA	Cone-beam CT	No	Yes	No	Yes	No	N/A	Yes	No	Yes	N/A
Parker et al[Paretal88]	1988	SBA & 3D Rec.	XRA	Yes	No	N/A	Yes	No	N/A	Yes	No	N/A	N/A
Sorantin et al [Soretal02]	2002	SBA & MMBA	Spiral CT	No	Yes	Yes	Yes	No	Yes	Yes	No	N/A	N/A
RIDGE-BASED APPROACHES													
Bullitt and Aylward[BulA01]	2001	RBA & SBA	MRA, CT & 3D-DSA	No	Yes	No	Yes	Yes	Yes	Yes	Yes	Yes	Yes
Guo and Richardson[GuoR98a]	1998	RBA	XRA	Yes	No	Yes	Yes	No	No	Yes	No	Yes	Yes
Aylward and Bullitt[AylB02]	2002	RBA	MRA, CT	No	Yes	No	Yes	Yes	Yes	Yes	Yes	Yes	Yes
Aylward et al[Ayletal96]	1996	RBA, MTLUDA	CT, MRA	No	Yes	No	Yes	No	Yes	Yes	Yes	Yes	Yes
REGION GROWING APPROACHES													
Schmitt et al[Schetal02]	2002	RGA	Rotational XRA	No	Yes	No	Yes	No	Yes	No	Yes	Yes	Yes
O'Brien and Ezquerro[OBrE94]	1994	RGA & SBA	XRA	Yes	No	Yes	Yes	No	Yes	Yes	No	Yes	Yes
Higgins et al[Higetal89]	1989	RGA	X-Ray CT	No	Yes	Yes	Yes	No	Yes	No	Yes	Yes	Yes
Yim et al[Yimetal00]	2000	RGA & SBA	MRA	No	Yes	Yes	Yes	No	Yes	Yes	Yes	Yes	N/A
Higgins et al[Higetal96]	1996	RGA & SBA	3D XRA	No	Yes	Yes	Yes	No	Yes	Yes	Yes	Yes	Yes
DIFFERENTIAL GEOMETRY-BASED APPROACHES													
Krissian et al[Krietal96]	1996	DGBA	MRA	No	Yes	No	Yes	No	N/A	No	Yes	Yes	N/A
Prinet et al[Prietal97]	1997	DGBA & SBA	DSA & MRA	Yes	Yes	No	No	No	No	Yes	Yes	Yes	Yes
Prinet et al[Prietal96]	1996	DGBA & SBA	MRA	No	Yes	No	No	No	No	Yes	Yes	Yes	Yes
Armande et al[Armetal99]	1999	DGBA, MSA & SBA	DSA & satellite images	Yes	No	Yes	Yes	Yes	N/A	Yes	No	Yes	Yes
MATCHING FILTERS APPROACHES													
Sato et al[Satetal98a]	1998	MFA	MRI, MRA, CT	No	Yes	Yes	Yes	Yes	N/A	No	Yes	Yes	Yes
Poli and Valli[PolV97]	1997	MFA & SBA	XRA	Yes	No	No	Yes	No	N/A	Yes	Yes	Yes	Yes
Hart et al[Haretal97b]	1997	MFA	Retinal img.	Yes	No	No	Yes	No	Yes	No	Yes	N/A	No
Wood et al[Wootetal95]	1995	MFA	Retinal img.	Yes	No	Yes	Yes	No	N/A	No	Yes	Yes	Yes
Hoover et al[Hooetal00]	2000	MFA	Retinal img.	Yes	No	No	Yes	No	N/A	No	No	Yes	Yes
Mao et al[Maoetal92]	1992	MFA & SBA	Subt. XRA	Yes	No	No	Yes	No	N/A	Yes	Yes	Yes	Yes
Chen et al[Cheetal98]	1998	MFA	XRA	Yes	No	No	Yes	No	No	No	Yes	Yes	No
MATHEMATICAL MORPHOLOGY SCHEMES													
Figueiredo and Leitao[FigL95]	1995	MMS	Nonsubt. XRA	Yes	No	No	Yes	No	Yes	No	Yes	No	No
Eiho and Qian[EihQ97]	1997	MMS & SBA	Coronarv XRA	Yes	No	Yes	Yes	No	Yes	Yes	Yes	Yes	Yes
Donizelli[Don98]		MMS & RGA	DSA	Yes	No	No	Yes	No	No	No	Yes	Yes	No
Zana and Klein[ZanK97]	1997	MMS & DGBA	Retinal XRA	Yes	No	No	Yes	No	No	No	Yes	Yes	Yes
Thackray and Nelson[ThaN93]	1993	MMS	DSA	Yes	No	Yes	Yes	No	Yes	No	Yes	Yes	N/A
DGBA : Diff. Geom.-based Approaches		MMS : Math. Morph. Schemes		RBA : Ridge-Based Approaches				RGA : Region Growing Approaches					
MFA : Matching Filters Approaches		MSA : Multi-Scale Approaches											
CT : Computed Tomography		MRI : Magnetic Resonance Im		XRA : X-Ray Angiography									
DSA : Digital Subtracted Angiography		MRA : Magnetic Resonance Angiogra											

Fig. 7. Comparison of the pattern recognition approaches.

internal and *external* forces, respectively. *Internal* forces serve to impose smoothness constraints on the contour while *external* forces pull the snake towards the desired image features like lines and edges.

We can represent the snake parametrically by $v(s) = (x(s), y(s))$, where $x(s)$ and $y(s)$ are coordinate functions and $s \in$

$[0, 1]$. The snake's total energy is:

$$E_{\text{snake}} = \int_0^1 E_{\text{snake}}(v(s)) ds. \quad (1)$$

The smoothness constraint imposed by *elasticity energy* makes the deformable models robust to the noise. The main

disadvantage is that usually it requires user interaction to initialize the snake. It also requires initial parameters given by the user. Automatic snake initialization is an active ongoing research topic [Caselles et al. 1993; Xu and Prince 1998].

Molina et al. [1998] use 3D snakes to reconstruct 3D catheter paths from biplane angiograms. First, geometric distortions in both images introduced by the X-ray projections of the vessels are corrected. This correction is achieved by finding and matching markers affixed to the input screens of both image intensifiers. Then a ridge detector is applied to segment the catheter in both images. The 3D snake used in this method is represented by B-splines and is initialized interactively. Using a snake facilitates the merging information from both projections simultaneously during the energy minimization process.

Rueckert et al. [1997] use deformable models in tracking of the aorta in cardiovascular MR images. The system tracks the shape of the aorta in a cardiac cycle to study *compliance*, which is a measure of elasticity of an artery and defined as the ratio of volume change per pressure change between contraction and expansion of the aorta. The location and diameter of the aorta is roughly estimated by using a multiscale medial response function accompanied with a priori knowledge about the circular shape of the aorta as an initial segmentation step. Then, the estimate obtained is refined using an energy minimizing Geometrically Deformable Model (GDM). Their work introduces two new aspects to the classical GDM. First, a Markov–Random Field (MRF) framework is introduced. The system uses Simulated Annealing (SA) and Iterated Conditions Modes (ICM) to minimize the energy of the snakes in the MRF framework. Second, GDM is represented by a spline-based representation which is C₂ continuous and has the advantage of computing the curvature from analytical models easily.

Kozerke et al. [1999] use a modified definition of the active contour models in their technique to automatically segment

vessels in cine phase contrast flow measurements. The method requires a user-selected vessel of interest in an arbitrary image frame. Then the system finds the phase image at the phase corresponding to the early systolic acceleration of blood flow as the starting frame. This is to ensure robust segmentation of the first image frame. In this frame, blood flow is expected to be unidirectional. The steps in this process are as follows: (1) Each phase frame is convolved with a Gaussian mask to reduce noise; (2) All pixels of each frame that exceed half of the maximum phase as found within a circular mask around the vessel center are detected; (3) Isolated pixels are removed and the holes are filled using connectivity information; and (4) The first phase image in time with an area of half of the maximum found overall is selected. The remaining frames are processed sequentially using the resulting contours of the previous frame as a model for the approximation of the contour in the current frame in case of missing or distorted edge features. The method uses phase image, in addition to the magnitude image, to handle image distortions.

Rueckert and Burger [1995] combine stochastic and probabilistic relaxation techniques in their adaptive snake model to segment vessels in cine MR images. It is assumed that the shape variation between successive time frames is relatively low. Based on this assumption, the method uses a Simulated Annealing (SA) stochastic relaxation technique to find the global energy minimum in the adaptive snake used to segment the vessel in the first frame. The subsequent frames are segmented using a fast probabilistic relaxation technique, called Iterated Conditional Modes (ICM). The segmentation results from previous frame is used to initialize the snake in the following frame. The adaptive snake is modeled as a 1D Markov Random Field (MRF) and is similar to the concept of Geometrical Deformable Models (GDMs) developed by Miller et al. [1991]. The method is tested with a volume of 16 256×256 MR images that cover the whole heart cycle. It is reported that the ascending as well

as the descending aorta have been located correctly.

Geiger et al. [1995] propose a method for detecting, tracking, and matching deformable contours. The method is based on the dynamic programming (DP) but it is noniterative and is guaranteed to find the global minimum. Detection algorithm creates a list of uncertainty points for each user-selected point. Then, a search window is created from two consecutive lists. Next, DP algorithm is applied to find the optimal contour passing through these lists. Deformable model is obtained after considering all possible contours and deformations. Since DP is slow and memory intensive, a multiscale approach is used to speed up the processing at the expense of losing the guaranteed optimality. In contour tracking process in consecutive frames, the contour obtained in the previous frame is sampled at high curvature points and these points form the initial points for the next frame. Matching, also based on DP, is achieved through a strategy developed which uses a cost function and some constraints. The method is applicable to a large spectrum of applications and the application to medical images is reported in the article.

Klein et al. [1994] use orientation specific filters together with B-Spline snakes to identify vascular features from angiogram images. The method consists of two major components: (1) A bank of orientation specific S-Gabor filter pairs are applied to create an image energy field; and (2) B-Spline snakes, representing the vessels, are employed to obtain centerline and edge features. Dynamic programming is used to optimize the B-spline snakes. The method is applied to a number of angiogram images, including pre and post-angioplasty coronary angiograms, and the results are reported. Due to the bank of orientation specific S-Gabor filter pairs used, this work can also be classified as a *matching filters* approach listed in Section 3.6.

McInerney and Terzopoulos [1997] describe Affine Cell Decomposition-based (ACD-based) deformable surfaces and show the potential use of these models

in extraction of complex structures from medical image volumes. Topologically deformable ACD-based models, called T-snakes and T-surfaces, are parametric models that embed deformable models in an ACD framework to extract very complex structures. 2D deformable models known as *topologically adaptable snakes*, *T-snakes*, are introduced in McInerney and Terzopoulos [1995]. Combining the ACD framework with deformable models allows the models to overcome the limitations of classical deformable models while keeping the traditional properties. A T-surface is defined as a closed oriented triangular mesh. The vertices of the triangles act as a dynamic particle system where the particles are connected by discrete springs. As the T-surface moves under the influence of internal and external energy forces, the model is reparameterized with a new set of triangles and nodes computed from the intersection points of the model with the superposed grid. Reparameterization of the model at every step allows the model to topologically transfer and adapt itself to more complex structures.

Klein et al. [1997] describe an approach to extract vessels from XRAs using deformable spline models. In their approach, user provides an initial estimate of the location of the vascular entity, and the system refines the estimate by deforming a snake, which is implemented by B-spline model. The energy function defines such constraints as the smoothness or coherence of the contour, the closeness of the contour to image edge pixels, and the compactness of the boundary. Gabor filter is used to determine the image energy term to attract the snake. The approach is most suitable for the accurate extraction of vascular segments. The amount of user interaction and computation required makes it impractical for extracting entire vascular structures. Due to the bank of orientation specific S-Gabor filter pairs used, this work can also be classified as a *matching filters* approach listed in Section 3.6.

Luo et al. [2000] design a model that overcomes the problems associated with traditional snakes, such as contour initialization, internal parameter setting, and

the limitations in the capture range of the external energy (EE). The model has new internal energy (IE) and new external energy that are treated equally. The internal energy maintains smoothness without any shrinking side effects on the contour. This is accomplished by computing “just enough” smooth force to overcome the image force. The external energy combines both edge and region information. This reduces the effects of contour initialization. The model was tested on both synthetic and real gray-level images and reported encouraging results.

Rueckert and Burger [1996] develop a technique based on geometrically deformable templates (GDT) to track and analyze cardiac MR images. The GDT model uses a bending energy term, in addition to image energy terms of classic deformable templates, to restrict the template to specific shapes. Any deformation of the template from its *equilibrium* shape requires this bending energy. The algorithm has two main steps: (1) Size, position, and orientation of the object is determined by affine transformations using only image energy; and (2) Shape is approximated by nonrigid deformations of the deformable template. The total energy of the template is minimized using a global optimization technique, Simulated Annealing (SA). The results of the algorithm applied to both MR cine sequences of the aorta and myocardium are reported.

Sarry and Boire [2001] propose a computer vision-based approach to track coronary arteries in biplane DSA images. They use a 3D contour model based on 3D Fourier shape descriptors and new constraints inferred from epipolar geometry. The 3D Fourier descriptors are obtained from 2D descriptors of the projected contour coordinates. A 3D parametrically deformable model is, then, employed in 3D tracking of the artery contours. The 3D tracking method developed is compared to classical 3D contour tracking method which consists of independent 2D tracking in each projection plane and 3D reconstruction using the epipolar geometry constraints. The model is reported to deal with calibration imperfections and

to show higher convergence rate and accuracy than the general 3D tracking method.

Toledo et al. [2000] combine a probabilistic principal component analysis technique (PPCAT) with a statistical snake (SS) technique to track non-rigid elongated structures. PPCAT is used to construct statistical image feature descriptions while snakes are used for global segmentation and to track objects. The SS learns and tracks image features using statistical learning techniques. A likelihood map, used by SS, is created from a training set of object profiles using the PPCAT. Each point in the map is assigned a probability measure to belong to the learned feature category. The likelihood map is extended, by applying an extended local coherence detection to the coherent direction field, to give priority to parallel coherent structures. The likelihood map is used to define a probabilistic potential field of the snake. The SS deforms itself to maximize the overall probability of detecting learned image features.

Hu et al. [1998] present a method based on global and local deformable physical models to extract vessel boundaries from MR cine phase-contrast (MR-CPC) images. The method uses a circular global model which fits the shape of the vessel cross-section boundary. The global model allows the method to detect vessel position and size changes in the time sequence of the phase-contrast images. Deformations on the global circular model is achieved through a local model. The local model, using variable stiffness parameters, locates the contour on the edge points while keeping the contour smooth at locations where edges are missing. Edge segments are extracted using directional gradient information. The algorithm was run on a set of over 500 MR-CPC images of the aorta from 20 patients and the results were reported to be very successful.

The work of Mayer et al. [1997] reviewed in Section 8 can be classified in this section due to ribbon-snakes used.

The work of Thackray and Nelson [1993] described earlier in Section 3.7 may be

thought of as model-based in that the 8 morphological operators are essentially explicit oriented vessel models.

The work of Hunter et al. [1995] reviewed in Section 7 can be classified as *parametric deformable model* due to the Knowledge-guided Snakes used in the extraction process.

The work of Parvin et al. [1994] reviewed in Section 8 can be classified in this section due to the deformed contour used.

The work of O'Donnell et al. [1994] reviewed in Section 4.3 can also be classified as a *parametric deformable model* approach due to the deformable surface used.

The work of Kompatsiaris et al. [2000] reviewed in Section 8 can also be classified as a *parametric deformable model* approach due to the active snakes used in refinement process of the detected stent.

4.1.2. Geometric Deformable Models and Front Propagation Methods. Caselles et al. [1993] and Malladi et al. [1995] use propagating interfaces under a curvature dependent speed function to model anatomical shapes. They use the Level Set Method (LSM) approach developed by Osher and Sethian [1988] and adapt it to shape recognition. The main idea behind the Level Set Method is to represent propagating curves as the zero level set of a higher dimensional function which is given in the Eulerian coordinate system. Hence, a moving front is captured implicitly by the level set function (LSF). The advantages of this approach are: (1) It can handle complex interfaces which develop sharp corners and change its topology during the development; (2) Intrinsic properties of the propagating front such as the curvature and normal to the curve can be easily extracted from the level set function; (3) Since the level set function is given in the Eulerian coordinate system, discrete grids can be used together with finite differences methods to obtain a numerical approximation to the solution; and (4) It is easily extendable to higher dimensions. Figure 8 shows the propagation of the front through a vessel in an angiogram image.

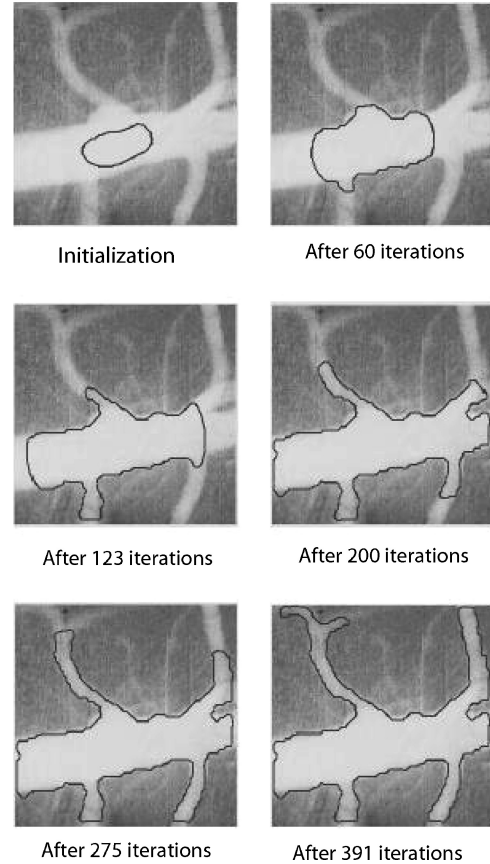


Fig. 8. Propagation of interface through a vessel in XRA image (Reproduced from Malladi et al. [1995]).

Sethian [1996] developed a computationally efficient Fast Marching Method (FMM), which uses a wave propagation approach for specialized front problems. FMMs are used in the problems where the front advances monotonically with a speed that does not change its sign. A good book on the Level Set Methods and Fast Marching Methods is written by Sethian [1999].

Quek and Kirbas [2001] and Quek et al. [2001] develop a wave propagation and traceback mechanism to extract vasculature from angiogram images. Using a dual-sigmoidal filter, the system labels each pixel in an angiogram with the likelihood that it is within a vessel. Representing the reciprocal of this likelihood image as an array of refractive indices, a digital wave is propagated through the

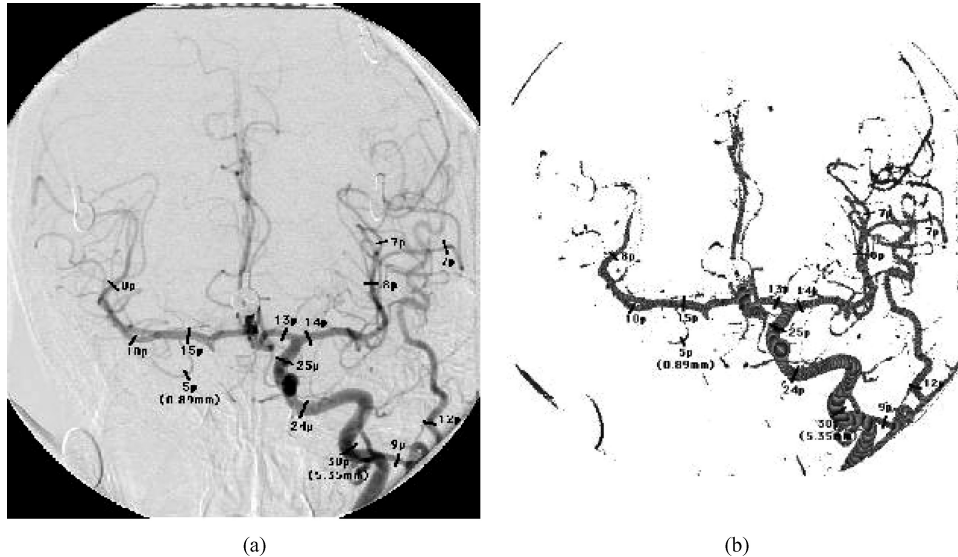


Fig. 9. (a) Original and (b) Wave propagated angiograms with measured vessel segments.

image from the base of the vascular tree. This wave ‘washes’ over the vasculature, ignoring local noise perturbations. The extraction of the vasculature becomes that of tracing the wave along the local normals to the waveform. While the approach is inherently SIMD, they present an efficient sequential algorithm for the wave propagation, and discuss the traceback algorithm. An example of wave propagation is shown in Figure 9. 3D wave propagation algorithm is discussed in Kirbas and Quek [2002]. Figure 10 shows the result of 3D wave propagation applied to a set of neurovascular MRI image with the interface created.

4.1.3. Deformable Template Matching Approaches. Template matching tries to recognize a structural model (template) in an image. The method uses the template as a *context*, which is a priori model. Thus, it is a *contextual method* and a *top-down* approach. In arterial extraction applications, the arterial tree template is usually represented in the form of a series of nodes connected in segments. This template is then deformed to fit the structures in the scene optimally. Stochastic deformation process described by a Hidden Markov

Model (HMM) is a method to achieve template deformation [Petrocelli et al. 1992, 1993]. Dynamic programming is an effective method employed in recognition process [Petrocelli et al. 1992].

Petrocelli et al. [1992] describe their method of structure recognition in unsubtracted digital angiograms. Their method, the *Deformable Template Matcher* is a combination of a priori knowledge of the arterial tree in the form of mathematical templates and a stochastic deformation process described by a Hidden Markov model (HMM). The structure model (template) is a set of connected nodes and their structural designations. The arterial tree is extracted by deforming the structure model and calculating the likelihood estimate of the deformation. The method uses dynamic programming technique in the recognition process.

Summers and Bhallerao [1995] implement a multiresolution technique based on octree representation for the segmentation of MRA. The image data is first expanded in an octree representation using averaging on the combined set of velocity component images. Image blocks, that pass the confidence test for the occupancy probability and coherence test for adjacency, form the segmented tree. The



Fig. 10. Extracted vessel tree using 3D wave propagation.

system estimates features like flow direction, vessel axis, diameter, and velocity from the segmented blocks using the local pressure gradient. The model is tested in extraction of vessels from MRA images and in calculation of pressure gradients in a model stenosis. Due to the multiscale approach used, we can list work under the *multiscale approaches* listed in Section 3.1.

van der Weide et al. [2001] localize paramagnetic markers to localize intravascular devices in MR images. The aim is to support the MR-guided vascular interventions. The method has two main steps: (1) Marker candidates, which are local minima ("blobs"), in the image are detected using both Laplacian image and *winding number image* [Kalitzin et al. 1998]. *Winding number image* is used to topologically classify different singular points such as local minima and local maxima points; and (2) The intravascular device is identified by a matching process of the detected marker pattern to the

known template of the device. The results of an animal experiment is discussed and a 95% success rate is stated in phantom experiments.

Petrocelli et al. [1993] present their method, based on a Gauss-Markov model, to recognize three dimensional vessel structures from biplane angiogram images. A unique feature of the system comes from its ability to extract structures from unprocessed standard digital angiograms without any preprocessing. The system, named Deformable Template Matcher (DTM), utilizes a priori knowledge of the arterial tree encoded as mathematical templates. An arterial tree template is represented in the form of a series of nodes connected in segments. This template is created by a cardiologist using an interactive mouse-driven program. This template is then deformed with a stochastic deformation process described by a Hidden Markov Model (HMM) to fit the unknown scene in the image using local image information. The template is

considered to fit the scene when the best of the state transition is found. Since the system is working in 3D, the deformation process is performed in space and back-projected onto two planes used. It requires a good model of the global structure and computational complexity to extract entire vascular structure.

4.2. Parametric Models (PM)

Parametric models approach defines objects of interest parametrically. In tubular object segmentation, objects are described as a set of overlapping ellipsoids. Some applications use a circular vessel model [Chan et al. 2000]. The parameters of the model used are estimated from the image. While an elliptic PM can approximate healthy vessels and stenoses, it fails to approximate pathological irregular shapes and vessel bifurcations. Pellet et al. [1994] employs deformable elliptic model to approximate irregular vessels and bifurcations.

Pellet et al. [1994] reconstruct vascular structures from two XRAs with an adapted simulated annealing algorithm. Healthy vessels and concentric stenoses are initially modeled using ellipses. This initial model is then deformed to fit to any branching cross-section or pathology. An adaptive simulated annealing optimization algorithm is used to control the deformation. Properties on the optimal solution are described by a Markov Random Field. The method is reported to perform well both on single vessels and on bifurcations.

Chan et al. [2000] utilize diameter information contained within the intensity profile *amplitude* (IPA) to estimate diameters of narrow vessels in X-ray cine-angiograms. A unique feature of the IPA is that it is sensitive to changes in small vessel diameters in case of noise and blur. The method has two steps: (1) Estimation of the imaging model parameters directly from the images and estimation of the diameters from these parameters. This step has three components to achieve imaging model parameters: a circular vessel model, a nonlinear imaging model, and a

parameter estimation. (2) Application of a maximum likelihood estimation technique with amplitude information incorporated. It is reported that the model successfully estimates the diameters in the range of 0.4 mm to 4.0 mm.

Krissian et al. [1998] develop a multiscale model to extract and reconstruct 3D vessels. The model is an extension of their previous work [Krissian et al. 1998a, 1998b]. It is based on previous work [Koller et al. 1995; Lorenz et al. 1997; Pizer et al. 1998; Fritsch et al. 1994, 1995; Lindeberg 1994, 1996], on multiscale detection with some modifications. It consists of three main steps: (1) Multiscale responses from discrete set of scales is computed; (2) Local extrema in multiscale response is extracted; and (3) Skeleton of the local extrema is created and the result is visualized. A cylindrical vessel model is utilized in the first step to interpret the eigenvalues of the Hessian matrix and to choose a good normalization parameter. The initial tests give promising results, with some local problems at vessel junctions and tangent vessels. Figure 11 shows some of the results of their work. An extension of this work, with a new response function, is reported in Krissian et al. [1999].

Bors and Pitas [1998] use a pattern classification-based approach for 3D object segmentation and modeling in volumetric images. The objects are considered as a stack of overlapping ellipsoids whose parameters are found using the normalized first and second order moments. The segmentation process is based on the geometrical model and gray-level statistics of the images. The center of the ellipsoids are estimated using an extended Hough Transform algorithm in 3D space. The method employs a radial Basis Function (RBF) network classifier in modeling the 3D structure and gray-level statistics. In the RBF classifier, each unit corresponds to an ellipsoid. The learning of the RBF network is based on the α -Trimmed Mean algorithm [Pitas and Venetsanopoulos 1990]. The algorithm was run on a set of tooth pulpal blood vessel microscopy images and the results were presented.

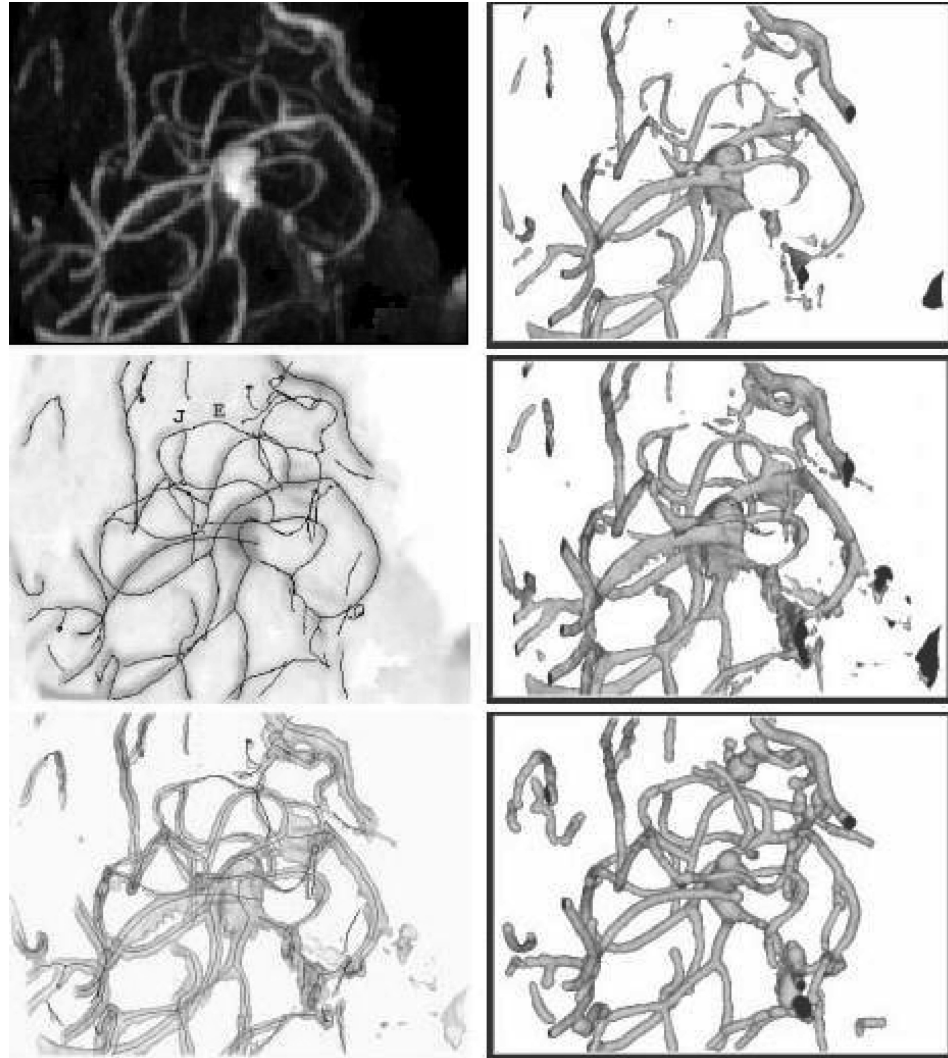


Fig. 11. **Left**, top to bottom, MIP of the original image, the detected centerlines superimposed on MIP, and the detected centerlines combined with an isosurface using transparency. **Right**, top to bottom, two isosurfaces of the initial image with different thresholds and an isosurface of the reconstructed image (Reproduced from Krissian et al. [1998a]).

4.3. Generalized Cylinders Model

Generalized cylinders (GC) are used to represent cylindrical objects. Technically generalized cylinders are parametric methods but we discuss them separately because there is a significant amount of work on this model and because of its prominence in the literature. Binford [1971] and Agin and Binford [1976] intro-

duced the use of GC in vision applications. Generalized cylinders consist of a space curve, or axis, and a cross-section function defined on that axis. The cross-section function is usually an ellipse. Tubular objects are defined by a cross-sectional element that is swept along the axis of the tube (spine) using some sweep rules. The spine is represented by a spline and the cross-section function is represented

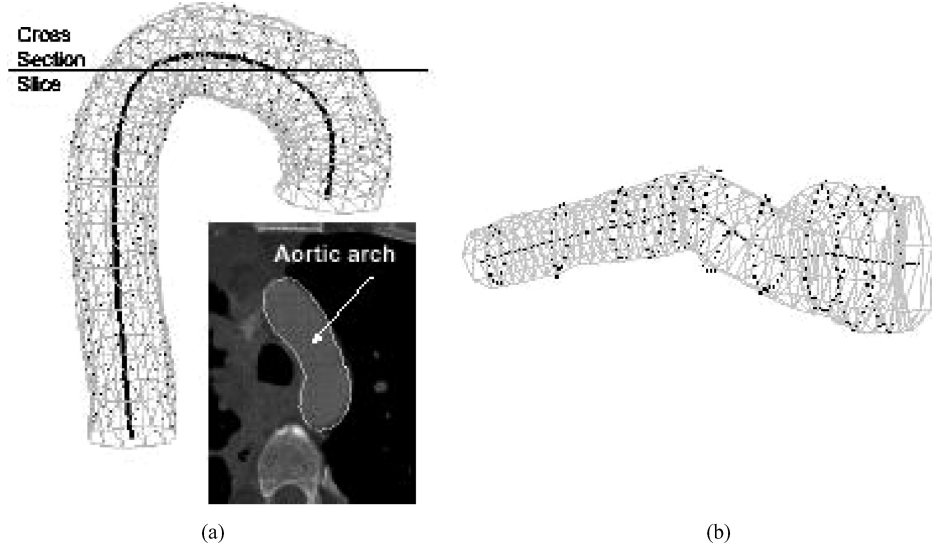


Fig. 12. (a) The final fit of the model to segmented CT angiogram of human aortic arch, and (b) Aorta with aneurysm (Reproduced from O'Donnell et al. [1997]).

by an ellipse. Another method to represent cylinders is to use Frenet-Serret formulation as the basis of generalized cylinders [Zerroug and Nevatia 1993]. However, Frenet-Serret formulation model and tube model described earlier suffer some serious drawbacks, such as discontinuities and non-intuitive twisting behavior. To alleviate these problems, researchers developed some other generalized cylinders models. One of these models is the *Extruded Generalized Cylinders (EGC)* developed by O'Donnell et al. [1994]. Their work is described in detail in this section.

Kayikcioglu and Mitra [1993] use a parametric model with elliptical cross-sections to reconstruct coronary arterial trees from biplane angiograms. Estimation of the vessel parameters are obtained from Marquardt-Levenberg technique which is a nonlinear least-square-error estimation technique. Kitamura et al. [1988a, 1988b] used a different version of the Marquardt-Levenberg technique in their work. Using these vessel parameters, elliptic model parameters are computed and used to reconstruct 3D artery segments. The authors report that their parametric modelling approach has better performance than those of the

derivative-based models particularly on consistency and variability.

O'Donnell et al. [1997] use a form of GC to recover cylindrical structures from medical images. A GC is a volume created by cross-section swept along a path, the spine. The spine is represented by a 3D cubic B-spline and the cross-section swept is always in the plane orthogonal to the spine to form the cylinder. The strength of their model comes from additional finite element (FEM) mesh-like component lying on top of their model to address the fine detail in complex structures. Figure 12 shows a result of their approach.

Sato et al. [1998a] propose a semi-automated method based on multiscale Hessian-based technique to determine the position, orientation, and diameter of stenoses in coronary angiograms. The Hessian matrix, H , describes the second-order structure of local intensity variations around each point in the image. The method consists of five stages: (1) Two images in which stenosis can be seen are selected; (2) corresponding points in two images are manually selected to find translational parameters; (3) 2D positions and orientations of the stenosis in two images are estimated; (4) 3D position and orientation of the stenosis are calculated

based on the principle of binocular stereo; (5) The vessel of interest with stenosis and any peripheral vessels which may be overlap the stenosis are specified manually. The method utilizes scale-dependency to formulate the diameter estimation to reduce user interaction.

Puig [1998a] describes her cerebral blood vessel modeling technique with a good imaging, modeling, and visualization review in her report. She proposes a hybrid model for the blood vessel representation scheme. The model stores symbolic information of the topology, such as branching and irregularities, like stenoses and aneurysms, as well as volume and surface information. The model uses graph representation associated with surface and volume information. Reconstruction of the symbolic model is achieved by extracting the Discrete Medial Axis (DMAT), described in Puig [1998b], based on a seed strategy that begins with a voxel of the medial axis and a main direction associated with the voxel. Each voxel is classified according to the projections of its wave and the graph is constructed incrementally. Associated surface model is created using Generalized Cylinders and volume model is created using run-length encoding.

Fessler and Macovski [1991] develop an object-based method for reconstructing arterial trees from a few projection images. The method uses an elliptical model of generalized cylinders to approximate arterial cross-sections. By incorporating a priori knowledge of the structure of arteries, the problem of reconstruction turns into an object estimation problem. The method employs a nonparametric optimality criterion that attempts to capture arterial smoothness incorporated in the system as a priori knowledge. The method was applied to three data sets and the results were reported.

O'Donnell et al. [1994] introduce a new deformable model, extruded generalized cylinder (EGC), for object segmentation. The article discusses the drawbacks of the existing generalized cylinder (GC) models and gives the rationale for their new model. The EGC model allows a nonplanar

spine and overcomes the problems caused by inflection points and spine torsion. The model has some properties that make it useful when there is no a priori curvature information about the object to be recovered: (1) Ability to describe cylinders with locally straight as well as curved spines; and (2) Having intuitive twisting behavior given by twisting parameters. The EGC model is further extended to include local surface deformations. The algorithm was applied to presegmented carotid artery data and the result was presented. This work can also be classified as a *parametric deformable model* approach listed in Section 4.1.1 due to the deformable surface used.

Kayikcioglu and Mitra [1992] analyze the shapes and calculate the areas of coronary arterial cross-sections from biplane angiograms using an elliptical model. The model uses ideal intensity distributions of an elliptical cross section of coronary artery to find the shape and area information. The method was tested on computer generated and real arterial data and the results were presented.

The work of Huang and Stockman [1993] reviewed in Section 8 can be listed in this section since they are using generalized cylinders to extract tubular structures in 2D intensity images.

4.4. 3D Reconstruction of Vessels

The works of Pellet et al. [1994] in Section 4.2, Krissian et al. [1998] in Section 4.2, Kayikcioglu and Mitra [1993] in Section 4.3, Puig [1998a] in Section 4.3, Fessler and Macovski [1991] in Section 4.3, and Molina et al. [1998] in Section 4.1.1 are related to 3D reconstruction of the vessels. A comparison table of papers reviewed in this section is given in Figure 13.

5. TRACKING-BASED APPROACHES

Tracking-based approaches apply local operators on a focus known to be a vessel and track it. On the other hand, pattern recognition approaches apply local operators to the whole image. Vessel tracking

Algorithm	Year	Classification	Input Type	Dimension 2D	Dimension 3D	Preprocessing	A priori Knowledge	Multi-scale Technique	User Interaction	Result Type			Whole Tree
										Centerline	Edges	Junctions	
PARAMETRIC MODELS													
Pellet et al[Peleta94]	1994	PM, 3D Recont.	XRA	Yes	Yes	No	Yes	No	No	No	Yes	Yes	No
Chan et al[Chetal00]	2000	PM	Cine XRA	Yes	No	No	Yes	No	No	No	Yes	N/A	N/A
Krissian et al[Krietal98a]	1998	PM, 3D Recont.	3D Med. Img.	No	Yes	No	Yes	Yes	Yes	Yes	N/A	Yes	Yes
Bors and Pitas[BorP98]	1998	PM	3D volumes	No	Yes	No	Yes	No	No	Yes	Yes	N/A	N/A
TEMPLATE MATCHING													
Petrocelli et al[Peteetal92]	1992	TM	Unsubt. XRA	Yes	No	No	Yes	No	No	Yes	No	Yes	No
Summers and Bhalerao[SumB95]	1995	TM & MSA	MRA	No	Yes	No	Yes	Yes	No	Yes	Yes	Yes	Yes
Weide et al[Weietal01]	2001	TM	MRI	Yes	No	Yes	Yes	No	Yes	Yes	N/A	N/A	N/A
Petrocelli et al[Peteetal93]	1993	TM	Biplane XRA	No	Yes	No	Yes	No	Yes	Yes	N/A	Yes	No
GENERALIZED CYLINDERS MODEL													
Kayikcioglu and Mitra[KayM93]	1993	GCM, 3D Reconst.	Biplane XRA	Yes	Yes	No	Yes	No	No	No	Yes	No	No
O'Donnell et al[O'Doetal97]	1997	GCM	CT of aorta	No	Yes	No	Yes	No	No	Yes	Yes	No	No
Sato et al[Satetal98b]	1998	GCM	XRA	Yes	Yes	Yes	Yes	Yes	Yes	Yes	No	No	No
Puig[Pui98a]	1998	GCM, 3D Reconst.	MRA, Spiral CTA	No	Yes	No	Yes	No	No	Yes	No	Yes	No
Fessler and Mackovski[FesM91]	1991	GCM, 3D Reconst.	MRA,	Yes	Yes	No	Yes	No	Yes	Yes	No	Yes	Yes
O'Donnell et al[O'Doetal94]	1994	GCM, PDM	Presegmented carotid artery	Yes	No	Yes	Yes	No	N/A	Yes	No	No	No
Kayikcioglu and Mitra[KayM92]	1992	GCM	Biplane XRA	Yes	No	No	Yes	No	N/A	Yes	No	No	No
PARAMETRIC DEFORMABLE MODELS													
Mollina et al[Moletal98]	1998	PDM, 3D Reconst.	Biplane XRA	Yes	Yes	Yes	Yes	No	Yes	No	Yes	N/A	N/A
Rueckert et al[Rueetal97]	1997	PDM	Spin-echo MRI	Yes	No	Yes	Yes	No	N/A	Yes	N/A	N/A	N/A
Kozeker et al[Kozetal99]	1999	PDM	MR Cine phase contrast	Yes	No	Yes	Yes	No	Yes	No	Yes	N/A	N/A
Rueckert and Burger[RueB95]	1995	PDM	Cine MRI	Yes	No	No	Yes	No	Yes	No	Yes	N/A	N/A
Geiger et al[Geietal95]	1995	PDM	Medical Images	Yes	No	No	Yes	Yes	Yes	Yes	Yes	N/A	N/A
Klein et al[Kleetal94]	1994	PDM, MFA	XRA	Yes	No	No	Yes	No	No	Yes	Yes	Yes	No
McInerney and Terzopoulos[Mc	1997	PDM	CT, MRI, MRA	No	Yes	No	Yes	No	Yes	No	Yes	Yes	Yes
Klein et al[Kleetal97]	1997	PDM, MFA	Coronary XRA	Yes	No	Yes	Yes	No	Yes	Yes	Yes	No	No
Luo et al[Luoetal00]	2000	PDM	Medical Images	Yes	No	No	Yes	No	Yes	No	Yes	Yes	No
Rueckert and Burger[RueB96b]	1996	PDM	Cardiac MRI	Yes	No	No	Yes	No	No	No	Yes	N/A	N/A
Sarry and Boire[SarB01]	2001	PDM	Biplane XRA	No	Yes	No	Yes	No	Yes	Yes	No	No	No
Toledo et al[Toletal00]	2000	PDM	XRA	Yes	No	Yes	Yes	No	Yes	Yes	No	No	No
Hu et al[Huetal98]	1998	PDM	MR Cine phase contrast	Yes	No	No	Yes	No	No	N/A	Yes	N/A	N/A

Fig. 13. Comparison of the model-based approaches.

(VT) approaches, starting from an initial point, detect vessel centerlines or boundaries by analyzing the pixels orthogonal to the tracking direction. Different methods are employed in determining vessel contours or centerlines. Edge detection operation followed by sequential tracing by incorporating connectivity information is a straightforward approach. Aylward et al. [1996] utilize *intensity ridges* to approximate the medial axes of tubular objects such as vessels. Some applications achieve sequential contour tracing by incorporating the features, such as vessel central point and search direction detected from previous step into the next step [Lu and Eiho 1993]. Fuzzy clustering is another approach to identify vessel segments. It uses linguistic descriptions like “vessel” and “nonvessel” to track vessels in retinal angiogram images. After the initial segmentation, a fuzzy tracking algorithm is applied to each candidate vessel region. Some methods utilize a model in the tracking process and incrementally segment the vessels. A more sophisticated approach on vessel tracking is the use of graph representation [Lecornu et al. 1994]. The segmentation process is, then, reduced to finding the optimum path in a graph representation of the image. One disadvantage of the vessel tracking approaches is that they are not fully automatic and require user intervention for selecting starting and end points.

Tolias and Panas [1998] develop a fuzzy C-means (FCM) clustering algorithm that uses linguistic descriptions like “vessel” and “nonvessel” to track fundus vessels in retinal angiogram images. Their

algorithm uses only (fuzzy) image intensity information and makes no assumptions for the shape of the vessels. First, optic nerve in fundus images is detected and used as the starting point. Next, the bounding circle of the optic nerve is found. Then, the points in the bounding circle are segmented as "vessel" and "nonvessel" using a FCM. Finally, a fuzzy vessel tracking algorithm is applied to each candidate vessel. The algorithm does not utilize any edge information to locate the vessels and this reduces the effects of noise in the tracking procedure.

Hart and Holley [1993] develop an automated coronary artery tracking system, which incorporates information within subsections of the image for stable tracking, in unsubtracted angiograms. The system iteratively operates on image blocks using a first order predictive scheme. Features obtained, such as vessel width and direction, from one image block (n), are input to next image block ($n + 1$) as initial information. Then, the system selects an appropriate image block size for an optimum width and direction for the next processing step. The seed direction, seed width and starting point of the first image block are given by user. This algorithm is relatively slow due to calculation being done on whole image blocks but faster than some tracking algorithms that use global image structures since it uses only local information in each image block. The system has problems in tracking arteries at bifurcations and sharp changes in vessel width.

Park et al. [1997] describe their work of extracting features and profiling narrow blood vessels in DSA images. Their system applies maximum-likelihood estimation on adjacent pixels for boundary detection and an adaptive tracking algorithm based on the direction field. The algorithm detects the position of centerlines as direction vectors and adaptively tracks entire vessel's direction field. A median filter is used as a preprocessing step to improve the image quality.

Quek et al. [1999, 2001] propose a model to interpret Neurovascular XRA images interactively. This attentionally-based in-

teractive model, AIM, exploits human interaction as part of the solution. AIM posits two channels of interaction: context ("what to look for"), and focus-of-attention ("where to look") as the locus of spatial information exchange between the user and the machine. In an AIM system, the user specifies a context (e.g., a carotid vessel) and directs the attentional spotlight to focus machine processing. AIM involves the user with the computer as integral partner and facilitates varying degrees of human intervention in the process. A hierarchy of context abstractions permits the system to function more autonomously (doing high-level tasks like extracting an arterial vessel) in routine interpretation, and to require more user intervention (e.g., locating arterial wall boundaries) as the image complexity increases. This feature lets the medical professional have ultimate control and confidence in the system. The system employs several edge detection algorithms, for example, Canny and Sobel, for the extraction of vessel boundaries.

Lu and Eiho [1993] describe their method of tracing the coronary arterial boundaries with sub-branches from XRAs. Their method has three steps: (1) Detecting edges; (2) Finding branches; and (3) Tracing contours sequentially. Edge points are evaluated and fixed by employing a smoothing differential operator on the scan line perpendicular to the direction of the vessel. Branch positions and branches are detected automatically from the same algorithm. Branching points are detected by checking the gray profile on the scan line. Sequential contour tracing achieved by incorporating the features, such as the central point, the searching direction, and the search range, detected from previous step into the next step. Initial central point, search direction, and search range is given by the user.

Ritchings and Colchester [1986] applied a syntactic pattern recognition scheme to diagnose vascular abnormalities. They process XRAs by applying an edge detector and pairing the resulting edge segments that may be parallel opposing edges of a vessel segment. These may be thought of as "ribbon segments" which may be

grouped to obtain extended vessel tracts. Each of these segments are labeled as *normal*, *widening*, *unsure*, and *abnormal* depending on the shape of the opposing edge segments using a syntactic pattern recognition system. The system does not attempt to determine the structure of the arterial system. The goal is to obtain these labels for the diagnosis of vascular abnormality.

Stockett and Soroka [1992] applied computer vision techniques to extract spinal cord contours from transaxial MR images. The method starts with the user supplying an approximate center point on the spinal cord. Then, the algorithm starts to search for edges by moving outwards along 16 equally spaced radials centered on the spinal cord. In case of lacking significant edges, an interpolation operation is performed on the radii. Finally, the extracted curve is smoothed by adjusting the edge points with respect to its neighboring edge points. The algorithm is fairly simple and runs on a personal computer but requires improvements on the edge detection and smoothing operations.

Lecornu et al. [1994] extract vessel contours in angiogram images by tracking two edges simultaneously by means of graph theory. A blood vessel model is incorporated and some blood vessel properties such as the position and size of section and the curvature of the segment are used in the formal structure model. The detection process employs a heuristic search method [Martelli 1976] which searches for the best edge in an image. The best edge is found as the optimum path in a graph representation of the image. They improve the algorithm by improving node concept by considering two opposite edges together to represent the vessel segments.

Chandrinos et al. [1998] extract vessels in fundus images for the examination of atherosclerotic changes due to hypertension. The method utilizes the idea that each vessel presents a ridge in cross-sectional intensity profiles. Ridge detection process starts with a Gaussian smoothing to handle the variations in image intensity. Then, a directional map is

built by registering the direction of the gradients at scanned image points. In the final image scan, ridge points are detected by suppressing pixels that do not satisfy a set of criteria, such as directional consistency with neighboring pixels, intensity supremacy over neighboring pixels, and contrast maximization in the direction orthogonal to the vessel direction. A set of filters is applied to the final image to clean the noise and repair fragmented vessels. After the extraction process, the method employs some image-based measuring techniques to obtain vessel caliber, wall thickness, and tortuosity.

Liu and Sun [1993] extract extended tracts of vasculature in XRAs by an adaptive tracking algorithm. Given an initial point within a vessel, they apply an “extrapolation update” scheme [Sun 1989] that involves the estimation of local vessel trajectories. Once a segment has been tracked, it is deleted in the angiogram image by growing the “deletion intensity value” over the grey levels representing the vessel. This procedure is performed recursively to extract the vascular tree. This algorithm requires user-supplied vessel starting points, and does not appear extensible to 3D extraction.

Haris et al. [1997b] develop an interactive method to extract vascular networks in angiograms. The method has five steps: (1) An adaptive smoothing process is applied using anisotropic diffusion which preserves the image structure; (2) Image gradient is calculated using the partial derivatives of the Gaussian filter; (3) Watershed transform is applied to the image gradient magnitude resulting in an initial partition image with many small homogeneous regions; (4) The resulting partition image is input to a fast region merging process; and (5) Vessel regions are extracted by a simple point-and-click interactive process. The segmented vascular network is represented by Region Adjacency Graph which provides spatial relationship information about the vessels in the network. The current version of the method works in 2D and it is reported that the smoothing algorithm used over-smooths the thin vessels.

Algorithm	Year	Classification	Input Type	Dimension		A priori Knowledge	Multi-scale Technique	User Interaction	Result Type		Whole Tree
				2D	3D				Centerline	Edges	
Tolias and Panas[TolP98]	1998	TBA	Retinal XRA	Yes	No	No	No	No	Yes	Yes	Yes
Hart and Holley[HarH93]	1993	TBA	Unsubt. XRA	Yes	No	No	No	Yes	No	Yes	No
Park et al[Paretal97]	1997	TBA	DSA	Yes	No	Yes	Yes	No	Yes	Yes	No
Quek et al[Queetal99]	1999	TBA	XRA	Yes	No	Yes	Yes	No	Yes	Yes	No
Quek et al[Queetal01a]	2001	TBA	XRA	Yes	No	Yes	Yes	No	No	Yes	Yes
Haris et al[Hareta97a]	1997	TBA	XRA	Yes	No	No	No	No	Yes	Yes	Yes
Lu and Eihol[LuE93]	1993	TBA	XRA	Yes	No	No	No	Yes	Yes	Yes	Yes
Ritchings and Colchester[RitC8]	1986	TBA	XRA	Yes	No	Yes	Yes	No	No	Yes	Yes
Stockett and Soroka[StoS92]	1992	TBA	MRI	Yes	No	No	Yes	No	Yes	Yes	No
Lecomte et al[Lecetal94]	1994	TBA	XRA	Yes	No	No	Yes	No	No	Yes	Yes
Chandrinos et al[Chaetal98]	1998	TBA & RBA	Retinal XRA	Yes	No	Yes	Yes	No	No	Yes	Yes
Liu and Sun[LiuS93]	1993	TBA	XRA	Yes	No	No	No	Yes	Yes	No	Yes
Haris et al[Hareta97b]	1997	TBA	DSA	Yes	No	Yes	No	No	Yes	Yes	Yes
Shen and Johnson[ShenJ94]	1994	TBA	XRA	Yes	No	Yes	Yes	No	Yes	No	N/A
Zhou et al[Zhoetal94]	1994	TBA	Retinal XRA	Yes	No	Yes	Yes	No	Yes	Yes	Yes
Stevenson et al[Steetal87]	1987	TBA	XRA	Yes	Yes	No	Yes	No	Yes	No	No

TBA : Tracking-Based Approach

RBA : Ridge-Based Approach

DSA :Digital Subtracted Angiography

XRA :X-Ray Angiography

Fig. 14. Comparison of the tracking-based approaches.

Shen and Johnson [1994] combine a conventional manual segmentation approach with a bimodal thresholding algorithm to develop a semi-automatic image segmentation tool. In the manual segmentation, user supplies control points of a cubic spline for each section and the system fits appropriate spline to these points. The automatic segmentation part applies a bimodal thresholding to the local window in the image given by the user. The steps of the algorithm are: (1) A starting point is entered by the user (2) An edge detection and contour following methods are applied to find region boundaries. Only a small piece is segmented at a time. Bimodal thresholding algorithm is used to determine the boundary segments in the local region; (3) User corrects any faulty contour; and (4) Algorithm continues to find the next segment. This approach works only in 2D images.

Zhou et al. [1994] develop a method to detect and quantify retinopathy in digital retinal angiograms. Their method relies on a matched filtering approach which uses a priori knowledge about retinal vessel properties. The tracking algorithm is an adaptive iterating procedure and models the vessel profile using Gaussian function. The algorithm also utilizes spatial continuity properties of the vessel segments to improve computational performance in regions where the vessel seg-

ments are relatively straight. This method requires the user to identify beginning and ending search points and first vessel direction manually.

Stevenson [1987] propose a system to track vessels between user-supplied vessel bifurcations. The uniqueness of their work is that they use vessel segments extracted from two different X-ray viewpoints to estimate 3D structure of the vasculature. The steps of the method are: (1) Bifurcation points in the first view and their corresponding points in the second view are entered by the user; (2) Vessel centerlines are tracked using local maxima; (3) Centerlines are smoothed and corrected; (4) 3D coordinates of centerline points in real space are calculated using transformation matrices; and (5) The next pair of images are loaded and the points marked in the previous frame are detected using statistical correlation technique. Algorithm repeats Steps (2) through (5) until the last frame. A comparison table of papers reviewed in this section is given in Figure 14.

6. ARTIFICIAL INTELLIGENCE-BASED APPROACHES

Artificial Intelligence-based approaches (AIBA) utilize knowledge to guide the segmentation process and to delineate vessel structures. Different types of knowledge

are employed in different systems from various sources. One knowledge source is the properties of the image acquisition technique, such as cine-angiography, DSA, computed tomography (CT), MRI, and MRA. Some applications utilize a general blood vessel model as a knowledge source. Smets et al. [1988] encode general knowledge about appearance of blood vessels in the form of 11 rules (e.g., that vessels have high intensity center lines, comprise high intensity regions bordered by parallel edges etc.). Stansfield [1986] applies a domain-dependent knowledge of anatomy to interpret cardiac angiograms in the high-level stages. According to Stansfield, "Anatomical knowledge is embodied within the system in the form of spatial relations between objects and the expected characteristics of the objects themselves". Knowledge-based systems exploit *a priori* knowledge of the anatomical structure. These systems employ some low-level image processing algorithms, such as thresholding, thinning, and linking, while guiding the segmentation process using high-level knowledge. AIBA perform well in terms of accuracy, but the computational complexity is much larger than some other methods.

Rost et al. [1998] describe their knowledge-based system, called Solution for a Learning Configuration System for Image Processing (SOLUTION), designed to automatically adopt low-level image processing algorithms to the needs of the application. It aims to overcome the problem of extensive change requirement in the existing system to perform in a different environment. The system accepts task descriptions in high-level natural spoken terms and configures the appropriate sequence of image processing operators by using expert knowledge formulated explicitly by rules. In the present implementation, extraction process is limited to contours.

Smets et al. [1988] present a knowledge-based system for the delineation of blood vessels on subtracted angiograms. The system encodes general knowledge about appearance of blood vessels in the form of 11 rules (e.g., that vessels have high

intensity center lines, high intensity regions bordered by parallel edges, etc.). These rules facilitate the formulation of a 4-level hierarchy (pixels, center lines, bars, and segments) each of which is derived from the preceding level by a subset of the 11 rules. The main stages in the algorithm are: (1) Obtain the center lines of the vessels by an adaptive maximum intensity detector; (2) Apply thresholding, thinning, and linking operations to get the final center lines segments; (3) Construct bar-like primitives using region growing algorithm on the center lines detected; and (4) Combine bar-like structures into vessel segments using geometrical and topological knowledge of the vessels. The system has considerable problems at vessel bifurcations and self-occlusions.

Stansfield [1986] describes a rule-based expert system, called ANGY, to segment coronary vessels from DSA images. There are three main stages in the ANGY system: a preprocessing stage which contains low-level image processing routines written in C and a rule-based expert system with two stages: a low-level image processing stage and a high-level medical stage. The former stage embodies domain-independent knowledge of segmentation, grouping, and shape analysis while the latter stage embodies a domain-dependent knowledge of cardiac anatomy and physiology. The system extracts vessel segments as trapezoidal units using an OPS5 production system. The rule set is used to determine which edge segments may participate to the formation of these trapezoidal strips and which segments arise from image noise. The system does not combine these units to form a vascular structure.

Goldbaum et al. [1996] describe their STARE (Structural Analysis of the Retina) image management system for the diagnosis and analysis of the retinal images. Segmentation of the images is achieved by employing rotating matched filters. After the extraction of the objects of interests, the classification is performed using one of the linear discrimination function, quadratic discrimination function, logic classifier, and back propagation artificial

Algorithm	Year	Classification	Input Type	Dimension		Preprocessing	A priori Knowledge	Multi-scale Technique	User Interaction	Result Type		Whole Tree
				2D	3D					Centerline	Edges	
Rost et al [Rosetal98]	1998	AIBA	Medical & Industr. Img.	Yes	No	Yes	Yes	No	No	N/A	Yes	N/A
Smets et al [Smeetal88]	1988	AIBA	Subtr. XRA	Yes	No	No	Yes	No	No	yes	Yes	Yes
Stansfield [Sta86]	1986	AIBA	DSA	Yes	No	Yes	Yes	No	No	Yes	Yes	No
Goldbaum et al [Goleta96]	1996	AIBA & MFA	Retinal XRA	Yes	No	No	Yes	No	No	No	Yes	Yes
Bombardier et al [Bometal97]	1997	AIBA	DSA	Yes	No	No	Yes	No	No	No	Yes	Yes

AIBA : Artificial Intelligence-Based Approaches

DSA : Digital Subtracted Angiography

MFA : Matching Filters Approaches

XRA : X-Ray Angiography

Fig. 15. Comparison of the artificial intelligence-based approaches.

neural networks with balanced accuracy and computation cost. Finally, the inferencing about the image content is accomplished with Bayesian network, which learns from sample images of the diseases. Due to the rotated matched filters used in the segmentation process, this work can also be classified as a *matching filters* approach listed in Section 3.6.

Bombardier et al. [1997] use two fuzzy segmentation operators for the automatic identification of artery boundaries from angiogram images in their knowledge-based approach. Different segmentation operators cooperate to extract different anatomical structures (the aorta and renal arteries). The segmentation process has two main steps: (1) Identification of the region of interest (ROI), which is the renal artery in this case; and (2) Detection of the boundaries of the identified structures automatically. They use fuzzy set theory to represent the knowledge. A comparison table of papers reviewed in this section is given in Figure 15.

7. NEURAL NETWORK-BASED APPROACHES

Neural networks are used to simulate biological learning and widely used in pattern recognition. Neural nets are basically a classification approach. The network is a collection of elementary processor (nodes). Each node takes a number of inputs, performs elementary computations, and generates a single output. Each node is assigned a weight and the output is a function of weighted sum of the inputs. These weights are learned through training and then used in the recognition.

Back-propagation algorithm is a widely used learning algorithm. One problem associated to learning is that, learning depends on the training data set. The size of the training data set effects the learning process. The training procedure should be rerun each time new training data is added to the set. Since the aforementioned neural networks require a training data set, the learning process is a *supervised learning*. A different class of neural networks are self-teaching and do not depend on training data set for the learning. The best known of these class of neural networks is Kohonen feature maps or Kohonen [1995] self-organizing networks. Interested readers are referred to Ripley [1996], Clak [1991], and Haykin [1994] for more information on neural networks. Neural networks are used in a wide range of applications. In medical imaging, neural networks are mainly used as a classification method where the system is trained with a set of medical images and the target image is segmented using the trained system. One of the advantages that make neural networks attractive in medical image segmentation is their ability to use nonlinear classification boundaries obtained during the training of the network. Another attractive feature is the ability to learn. With the selection of a good training set which includes all possible features or objects, the network can learn the classification boundaries in its feature space. One of the disadvantages of neural networks is that they need to train every time a new feature is introduced the network. Another limitation is the difficulty of debugging the performance of the network.

Cronemeyer et al. [1992] describe their skeleton finder which is a parallel version of the work done by Nguyen and Sklansky [1986a, 1986b]. Their work aims to reconstruct vessels in 3D from biplane angiograms. The algorithm starts with a segmentation process to reduce the region to search artery-like structures. Then, ridges and boundaries are detected in the segmented regions. Next, vessel segments are tracked in parallel. They implemented an adaptive tracking as well as a standard tracking algorithm and compared the results. It is stated that the adaptive tracking algorithm is less sensitive to artifacts and erroneous ridge points while standard algorithm performs better tracking of small and noisy segments. Finally, all detected vessels are combined to form the artery tree. Due to the ridge detection performed, this work can also be classified as a *ridge-based* approach listed in Section 3.3.

Nekovei and Sun [1995] detect blood vessels in XRA images using neural networks with back-propagation algorithm. This system does not extract the vascular structure. Its purpose is to label the pixels as vessel or non-vessel. The system applies neural network directly to the image pixels without prior feature detection. Since angiograms are typically very large, the network is applied to a small subwindow which slides across the angiogram. Pixels of this subwindow are directly input to the network. Prelabeled angiograms are used to train the network. The algorithm is compared with two other algorithms, *bayesian maximum likelihood algorithm* and *iterative ternary classification algorithm* [Kottke and Sun 1990b], and the classification accuracy of three methods are compared.

Hunter et al. [1995] combine neural network-based approach with knowledge-guided snakes to extract Left Ventricular (LV) boundaries in Echocardiographic images. Their method comprises three stages. In first two stages, neural network-based radial search algorithm detects candidate LV edge points along a set of radial search lines which define the polar domain. The final boundary extrac-

tion takes place in this polar domain. In the third stage, Knowledge-guided Snakes automatically select LV boundary points from the candidate edge points. They develop a new two stage Dynamic Programming method reported to be faster than the original method in their snakes implementation. Due to the Knowledge-guided Snakes used in the extraction process, this work can also be classified as a *parametric deformable model* approach listed in Section 4.1.1.

Kottke and Sun [1990b] apply an iterative ternary classifier and learning process to extract arterial structures in coronary angiograms. Their algorithm initially classifies the image as “artery”, “background” and “undecided”. Then, a two step iterative process is employed to adjust the threshold to further classify the “undecided” pixels. Threshold adaptation is governed by a learning algorithm based on the line and consistency measurements around the pixels. The performance of the algorithm is compared to two other general purpose segmentation algorithms, a *relaxation algorithm* developed by Rosenfeld and Smith [1981], and a *scattering-based approach* developed by Otsu [1979].

Shiffman et al. [1996] combine an automated neural network-based segmentation approach with manual editing to extract sections from computed tomography angiography (CTA) image volumes. They aim to facilitate the visualization of vasculature by editing the target sections in the volume prior to 3D reconstruction. The first step of the method involves an automatic segmentation of an entire image sequence of CTA sections which produces a set of labelled image sections. The next step requires the user to view the resulting images and edit one or more sections. In the final step, user edited segments and the remaining section are connected to extract the final image segments based on label identity. Automated segmentation is achieved in two steps; a multilevel thresholding and then smoothing the resulting fuzzy regions. Two clustering methods, *K-means clustering algorithm* and a *neural network-based algorithm* based on

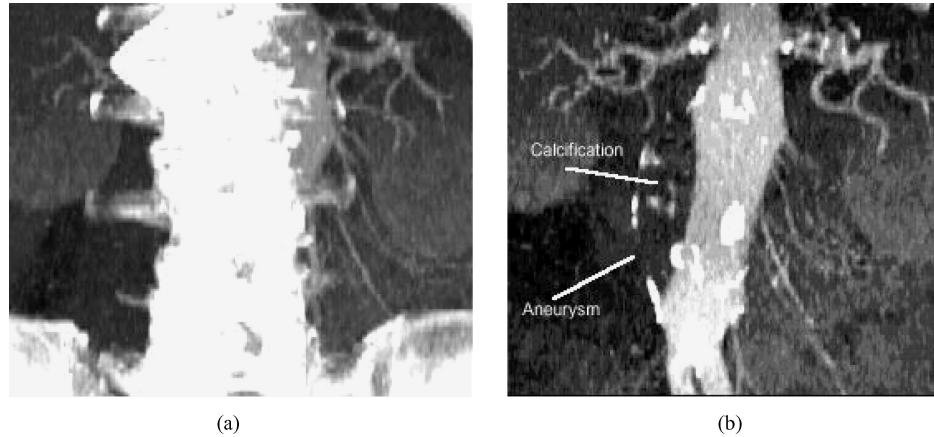


Fig. 16. (a) MIP of the CTA data set, and (b) MIP of the spine extracted using conventional connectivity (Reproduced from Schiffman et al. [1996]).

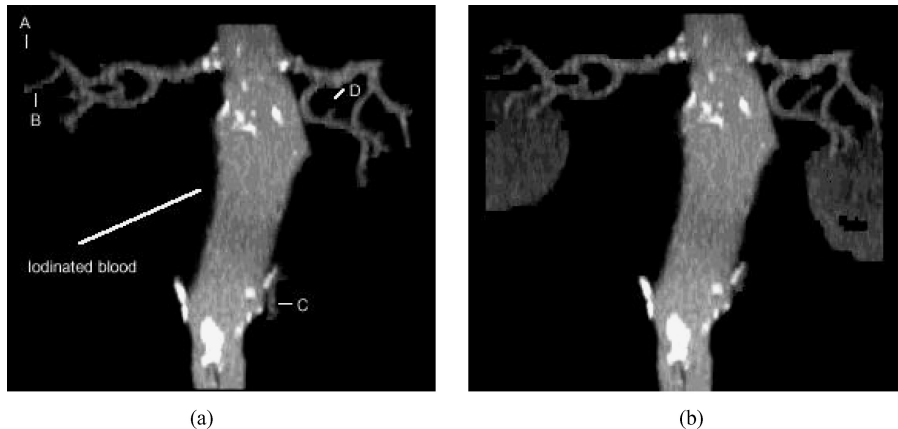


Fig. 17. (a) MIP of the aorta via conventional connectivity, and (b) MIP of the aorta extracted using the developed method (Reproduced from Schiffman et al. [1996]).

Kohonen's self-organizing feature maps, has been implemented and the results are compared.

Figures 16 and 17 show maximum intensity projections (MIP) of complete data set and the results produced by conventional connectivity and the method developed.

7.1. 3D Reconstruction of Vessels

The works of Cronemeyer et al. [1992] and Schiffman et al. [1996] are related to 3D reconstruction of the vessels. A comparison table of papers reviewed in this section is given in Figure 18.

8. TUBE-LIKE OBJECT DETECTION APPROACHES

This class of research approaches deals with the extraction of tubular structures from images. This is actually a "miscellaneous" class of approaches that may be applicable to vascular extraction in that vessels are tubular entities, but these approaches were not designed for vessel extraction per se.

Davies [1987] develops a system to locate circular objects to be used in industrial automation. His system aims to emulate standard Hough transform technique and is claimed to work faster. The standard Hough transform to locate round

Algorithm	Year	Classification	Input Type	Dimension		Preprocessing	A priori Knowledge	Multi-scale Technique	User Interaction	Result Type		Whole Tree
				2D	3D					Centerline	Edges	
Cronemeyer et al [Croetal92]	1992	NNBA & 3D Reconstr.	Biplane XRA	Yes	Yes	No	Yes	No	No	Yes	Yes	Yes
Nekovei and Sun [NekS95]	1995	NNBA	XRA	Yes	No	No	Yes	No	No	No	No	Yes
Hunter et al [Hunetal95]	1995	NNBA & PDM	Echocardiography	Yes	No	No	Yes	Yes	No	N/A	Yes	N/A
Kottke and Sun [KotS90b]	1990	NNBA	Coronary XRA	Yes	No	No	Yes	No	No	No	No	Yes
Shiffman et al [Shietal96]	1996	NNBA & 3D Reconstr.	CTA	Yes	Yes	No	No	No	Yes	No	No	N/A

NNBA : Neural Net-Based Approach

PDM : Parametric Deformable Model

CTA : Computed Tomography Angiography

XRA : X-Ray Angiography

Fig. 18. Comparison of the neural network-based approaches.

objects employs an edge detector. The resulting edge information is used to find candidate center locations. Finally, candidate center locations are averaged to obtain an estimate of the position of the object's center. These operations are costly for the industrial application domain. Davies' technique employs image sampling and a very small neighborhood to improve the speed. The strategy requires two passes over the image to determine the center location. The divisions, multiplications and square root calculations are replaced by 2-element averaging operations to reduce computation.

Grimson et al. [1993] observe that cylindrical objects in 3D range images appear as conic profiles along the scan lines. They use a conic detector to detect such profiles and extract tubular objects from range images obtained from an active structured-light laser scanner. Their approach consists of five steps: (1) Location and orientation of cylindrical tube segments are hypothesized in world coordinate to get rough estimate of the tube position; (2) The hypotheses are matched against tube model to get an estimate of the position and orientation of the whole tube; (3) A scanning path is planned to trace the whole tube; (4) A tube model is created by scanning the tube in detail at close range, which gives high accuracy information; and (5) The created tube model is matched to the model used and the deficiencies in the detected tube are reported.

Mayer et al. [1997] develop a model for the extraction of roads from aerial images. Their model has three basic components. First, a multiscale modeling is used

**Fig. 19.** Extracted roads from an aerial image (Reproduced from Mayer et al. [1997]).

to combine fine scale detailed information such as road markings, with coarse scale abstract information such as the road network. Second, context information in the form of relations to other objects such as buildings and trees is exploited to extend the model. This facilitates the extraction process to focus on the target objects. Third, ribbon-snakes are used to extract roads in fine scales. Using ribbon-snakes is reported to help the extraction of the roads occluded by shadows cast by buildings and trees in the image. Figure 19 shows extracted roads in an aerial image. Due to the ribbon-snakes used, this work can also be classified as a *parametric deformable model* listed in Section 4.1.1. This work is also a multiscale approach listed in Section 3.1.

Kompatsiaris et al. [2000] detect boundaries of stents in angiographic images. Their method first constructs a training

set using perspective projection of various deformations of the 3D wireframe model of the stent. Initial detection of the stent is accomplished by using the training set for deriving a multivariate Gaussian density estimate based on eigenspace decomposition using Principal Component Analysis (PCA). Then, a maximum likelihood estimation framework is formulated to extract the stent. Finally, a 2D active contour model (snake) is used to refine the detected stent. Initialization of the snake is accomplished by an iterative technique considering the geometry of the stent. This work can also be classified as a *parametric deformable model* listed in Section 4.1.1 due to the active snakes used in refining the detected stent.

Thirion et al. [2000] incorporate high level constraints and user feedback to overcome some of the drawbacks that traditional image segmentation methods face in complex environments. Their system aims to segment pipelines in industrial images. They try to handle the challenges due to shading, highlights, and textual variations by fusing physics-based vision, edge and texture analysis, probabilistic learning, and the graph-cut formalism methods. The parameters of the physics-based model of color and highlights of the pipes are learned from a set of training windows selected by user from input images. Next, a bank of filters to detect features like color/highlight, contour, and shading/anisotropy are applied to the image. A probabilistic graph which describes the image is built from the output of the previous step. Finally, segmentation is performed by using graph cut method. Segmentation can be improved through user feedback into the graph. This work can also be classified as a *matching filters* approach listed in Section 3.6 due to the bank of filters used in segmentation process.

Huang and Stockman [1993] describe a system that uses *generalized cylinders* to extract tubular structures in 2D intensity images. The system combines contour-based and shading-based methods and uses a 3D tube model. These cylinders are defined by a cross-sectional element

that is swept along the axis of the tube using some sweep rules. There are two main stages in the algorithm: local recognition stage and global recognition stage. The first step in the local recognition stage is the detection of reliable contour primitives. These primitives provide constraints for the localization of the tubes. Next, optimal filters are generated dynamically and matched against the data in order to verify the shading property of the tubes under detection. In the global recognition stage, locally verified tubes from the first stage are used as seeds and are swept along the axis of the tube using some sweep rule using best fit constraint. The key issue is to control the smoothness of the sweeping. Huang and Stockman [1993] shows results of this algorithm applied to the extraction of tree roots.

This work can also be classified as a *generalized cylinders* model listed in Section 4.3 due to the generalized cylinders model used. We can also put this work under the *matching filters approach* listed in Section 3.6 due to the matched filters used in the segmentation process.

Parvin et al. [1994] develop a technique for detection, tracking, and representation of tubular objects in images. In this technique, at the macro level, geometric properties are used to localize and to track the objects and at the micro level, high and low-level constraints are used to model the detection and tracking the subsystems. In the object detection process, perceptually significant features from the image are extracted and used as high-level cues in refining the object boundaries. The result of their approach is shown by an implementation that detects and tracks DNA molecules obtained through epifluorescence microscopy. High-level cues in the application domain are ribbon-like structures defined by a collection of substructures called “U-shapes” and anti-parallel segments. These isolated segments are grouped with respect to the object model in terms of a bounding polygon. This global representation is then refined using local pixel activities. Dynamic programming is employed in the refinement process. The refined contour is projected

Algorithm	Year	Classification	Input Type	Dimension 2D	Dimension 3D	Preprocessing	A priori Knowledge	Multi-scale Technique	User Interaction	Result Type		Whole Tree
										Centerline	Edges	
Davies[Dav87]	1987	MTLODA	Gray-level	Yes	No	No	Yes	Yes	No	N/A	N/A	N/A
			Industr. Img.									
Grimson et al [Grietal93]	1993	MTLODA	Range Images	No	Yes	No	Yes	No	No	N/A	N/A	N/A
Mayer et al[Mayetal97]	1997	MTLODA , PDM & MSA	Aerial Images	Yes	No	No	Yes	Yes	No	Yes	Yes	N/A
Kompatsiaris et al[Kometal00]	2000	MTLODA & PDM	XRA	Yes	No	No	Yes	No	No	N/A	Yes	N/A
Thirion et al[Thietal00]	2000	MTLODA & MFA	Industr. Img.	Yes	No	No	Yes	No	Yes	N/A	N/A	N/A
Huang and Stockman[HuaS93]	1993	MTLODA, MFA & GCM	Different Application Domains	Yes	Yes	No	Yes	No	No	No	Yes	N/A
Parwin et al[Pareta94]	1994	MTLODA & PDM	Epi-fluorescence Microscopy of DNA molecules	Yes	No	Yes	Yes	No	No	Yes	Yes	N/A

GCM: Generalized Cylinders Model
MSA : Multi-Scale Approaches

MTLODA : Miscellaneous Tube-Like Object .Detection Approaches
PDM : Parametric Deformable Model

Fig. 20. Comparison of the tube-like object detection approaches.

and updated in every consecutive frame to track the object in a time sequence of images. The system also provides an axis of symmetry representation of object for subsequent scientific analysis.

This system has some limitations. First, the detection subsystem is dependent on the correct computation of local symmetries. The system is unable to probe the image further and to infer additional missing local symmetries. Next, the tracking subsystem assumes that the normal lines to the smooth polygon intersect the actual boundary of the object. The system has difficulty with rapidly deforming objects. Finally, shape representation is based on finding the end points of the object which are hypothesized by the curvature peaks along the contour. Due to the noise, these peaks may not be locally accurate.

This work can also be classified as a *Parametric deformable model* listed in Section 4.1.1. A comparison table of papers reviewed in this section is given in Figure 20.

9. CONCLUSION

Segmentation algorithms form the essence of medical image applications such as radiological diagnostic systems, multimodal image registration, creating anatomical atlases, visualization, and computer-aided surgery. Even though many promising techniques and algorithms have been developed, it is still an

open area for more research. The future direction of segmentation research will be towards developing faster and more accurate more automated techniques.

Fast advances in radiological imaging systems result in high volume patient images. Processing of these images in radiological diagnostic systems requires fast segmentation algorithms. One way to achieve faster segmentation results is to develop parallel algorithms. Cronemeyer et al. [1992] exploit the parallel nature of the hardware and develop a fast skeleton finder algorithm. Neural network-based approaches also achieve faster segmentation due to their parallel nature. Another approach to achieve faster segmentation is to employ multiscale processing technique in which major structures are extracted using low-resolution images while fine structures are extracted using high-resolution images.

Another way to achieve fast processing of radiological images is to exploit the developments in the current technology which produces high speed processors with less cost. One can create a farm of computer systems and let each system process an image at a time. This will result in parallel processing of images using a sequential algorithm.

Accuracy of the segmentation process is crucial due to the nature of the work and is essential to achieve more precise and repeatable radiological diagnostic systems. Accuracy can be improved by incorporating *a priori* information on vessel anatomy

and letting high level knowledge guide the segmentation algorithm.

Even though expert knowledge and guidance is essential in segmentation systems, sheer volume of the medical image data requires more automatic segmentation systems to reduce the work load.

We provide a survey of current vessel segmentation methods. We have tried to cover both early and recent literature related to vessel segmentation algorithms and techniques. Our aim was to introduce the current segmentation techniques. We intended to give the practitioner a framework for the existing research and to introduce interested parties to the panoply of vessel segmentation literature. We will continue to update this review with new references and will post it on vislab.cs.vt.edu/review/extraction.html web address.

REFERENCES

- AGIN, G. AND BINFORD, T. 1976. Computer description of curved objects. *IEEE Trans. Comput. C-25*, 439–449.
- ARMANDE, N., MONGA, O., AND MONTESINOS, P. 1995. Extraction of thin nets in grey-level images. In *Proceedings of Scandinavian Conference on Image Analysis*. 287–295.
- ARMANDE, N., MONTESINOS, P., AND MONGA, O. 1999. Thin nets extraction using multi-scale approach. *Comput. Vis. Image Understand.* 73, 2, 248–257.
- AYACHE, N. 1994. Medical computer vision, virtual reality and robotics. *Image Vis. Comput.* 13, 4, 295–313.
- AYACHE, N., GUÉZIEC, A., THIRION, J., AND GOURDON, A. 1993. Evaluating 3-d registration of ct-scan images using crest lines. *Math. Meth. Med. Imag. II* 2035, 06 (July), 60–71.
- AYLWARD, S. AND BULLITT, E. 2001. Analysis of the parameter space of a metric for registering 3d vascular images. In *Proceedings of the International Conference on Medical Image Computing and Computer-Assisted Intervention*.
- AYLWARD, S. AND BULLITT, E. 2002. Initialization, noise, singularities, and scale in height ridge traversal for tubular object centerline extraction. *IEEE Trans. Med. Image.* 21, 2 (Feb.), 61–75.
- AYLWARD, S., JOMIER, J., WEEKS, S., AND BULLITT, E. 2002. Registration and analysis of vascular images. *Int. J. Comput. Vision.*
- AYLWARD, S., PIZER, S., BULLITT, E., AND EBERL, D. 1996. Intensity ridge and widths for tubular object segmentation and description. In *Proceedings of the Workshop on Math. Methods in Biomed. Image Analysis*. 131–138.
- BINFORD, T. 1971. Visual perception by computer. In *IEEE Conf. on Sys. and Controls*.
- BOMBARDIER, V., JALUENT, M., BUBEL, A., AND BREMONT, J. 1997. Cooperation of two fuzzy segmentation operators for digital subtracted angiograms analysis. In *IEEE Conference on Fuzzy Systems*. Vol. 2. 1057–1062.
- BORS, A. G. AND PITAS, I. 1998. Object segmentation and modeling in volumetric images. In *Proc. Wksp on Non-Linear Model Based Image Analysis*. 295–300.
- BUHLER, K., FELKEL, P., AND LA CRUZ, A. 2002. Geometric methods for vessel visualization and quantification—A survey. Tech. Rep. TR_VRVis_2002_035, VRVis Research Center, Vienna, Austria.
- BULLITT, E. AND AYLWARD, S. 2001. Analysis of time-varying images using 3d vascular models. In *Proc. Applied Imagery Pat. Recog. Works.* 9–14.
- BULLITT, E., AYLWARD, S., LIU, A., STONE, J., MUKHERJI, S., COFFEY, C., GERIG, G., AND PIZER, S. 1999. 3d graph description of the intracerebral vasculature from segmented mra and test of accuracy by coparisons with x-ray angiograms. *Inf. Proc. Med. Imag.* 1613, 308–321.
- BULLITT, E., AYLWARD, S., SMITH, K., MUKHERJI, S., JIROUTEK, M., AND MULLER, K. 2001. Symbolic description of intracerebral vessels segmented from MRA and evaluation by comparison with x-ray angiograms. *IEEE Med. Image Anal.* 5, 157–169.
- CANNY, J. 1983. Finding edges and lines in images. Tech. Rep. 720, MITAI.
- CASELLES, V., CATTE, F., COLL, T., AND DIBOS, F. 1993. A geometric model for active contours in image processing. *Numer. Math.* 66, 1, 1–32.
- CHAN, R., KARL, W., AND LEES, R. 2000. A new model-based technique for enhanced small-vessel measurements in x-ray cine-angiograms. *IEEE Trans. on Med. Image* 19, 3 (March), 243–255.
- CHANDRINOS, K. V., PILU, M., FISHER, R. B., AND TRAHANIAS, P. E. 1998. Image processing techniques for the quantification of atherosclerotic changes. In *Mediterranean Conf. Medical and Bio. Eng. and Computing*.
- CHAUDHURI, S., KATZ, N., NELSON, M., AND GOLDBAUM, M. 1989. Detection of blood vessels in retinal images using two dimensional blood vessel filters. *IEEE Trans. on Med. Img.* 8, 3 (Sept.).
- CHEN, J., SATO, Y., AND TAMURA, S. 1998. Orientation space filtering for multiple orientation line segmentation. In *Proc. of the IEEE Conf. on CVPR*. 311–317.
- CHEN, J., SATO, Y., AND TAMURA, S. 2000. Orientation space filtering for multiple orientation line segmentation. *PAMI* 22, 5 (May), 417–429.
- CHEN, Q., STOCK, K., PRASAD, P., AND HATABU, H. 1999. Fast magnetic resonance imaging techniques. *European J. of Radio.* 29, 2 (Feb.), 90–100.
- CHWIAŁKOWSKI, M., IBRAHIM, Y., HONG, F., AND PESHOCK, R. 1996. A method for fully automated

- quantitative analysis of arterial flow using flow-sensitized MR images. *Comp. Med. Imaging and Graphics* 20, 5, 365–378.
- CLAK, J. 1991. Neural network modelling. *Physics in Med. and Bio.* 36, 1259–1317.
- CLARKE, L., VELTHUIZEN, R., CAMACHO, M., HEINE, J., VAIDYANATHAN, M., HALL, L., AND THATCHER, R. 1995. MRI segmentation: Methods and applications. *Magne. Reson. Imaging* 13, 3, 343–368.
- COTE, B., HART, W., GOLDBAUM, M., KUBE, P., AND NELSON, M. 1994. Classification of blood vessels in images of the ocular fundus. Tech. Rep. CS94-350, UCSD.
- CRONEMEYER, J., HEISING, G., AND ORGLMEISTER, R. 1992. A fast skeleton finder for parallel hardware. In *IEEE Computers in Cardiology*. 23–26.
- DAVIES, E. 1987. A high speed algorithm for circular object detection. *Pattern Rec. Let.* 6, 323–333.
- DO CARMO, M. 1976. *Differential geometry of curves and surfaces*. PH.
- DONIZELLI, M. 1998. Region-oriented segmentation of vascular structures from dsa images using mathematical morphology and binary region growing. In *Proc. of the Works. Image Proces. for the Medicine*. Vol. 12.
- DUNCAN, J. S. AND AYACHE, N. 2000. Medical image analysis: Progress over two decades and the challenges ahead. *PAMI* 22, 1 (Jan.), 85–105.
- EIHO, S. AND QIAN, Y. 1997. Detection of coronary artery tree using morphological operator. *IEEE Comput. Cardiol.* 24, 525–528.
- FELKEL, P., WEGENKITT, R., AND KANITSAR, A. 2001. Vessel tracking in peripheral CTA datasets—An overview. In *Spring Conf. on Computer Graph.* 232–239.
- FESSLER, J. A. AND MACOVSKI, A. 1991. Object-based 3-d reconstruction of arterial trees from magnetic resonance angiograms. *IEEE Trans. on Med. Image* 10, 1 (Mar.), 25–39.
- FIGUEIREDO, M. AND LEITAO, J. 1995. A nonsmoothing approach to the estimation of vessel contours in angiograms. *IEEE Trans. on Med. Image* 14, 162–172.
- FRITSCH, D., EBERLY, D., PIZER, S., AND McAULIFFE, M. 1995. Simulated cores and their application in medical imaging. *Inf. Proc. Med. Imaging*, 365–368.
- FRITSCH, D., PIZER, S., MORSE, B., EBERLY, D., AND LIU, A. 1994. The multiscale medial axis and its applications in image registration. *Pattern Rec. Let.* 15, 5, 445–452.
- GEIGER, D., GUPTA, A., COSTA, L., AND VLONTZOS, J. 1995. Dynamic programming for detecting, tracking, and matching deformable contours. *PAMI* 17, 3, 294–302.
- GOLDBAUM, M., MOEZSI, S., TAYLOR, A., CHATTERJEE, S., BOYD, J., HUNTER, E., AND JAIN, R. 1996. Automated diagnosis and image understanding with object extraction, object classification, and inferencing in retinal images. In *IEEE Int. Conf. on Image Processing*. Vol. 3.
- GRIMSON, W., LOZANO-PEREZ, T., NOBEL, N., AND WHITE, S. 1993. An automatic tube inspection system that finds cylinders in range data. In *Proc. of the IEEE Conf. on CVPR*. 446–452.
- GUÉZIEC, A. AND AYACHE, N. 1994. Smoothing and matching of 3-d space curves. *Int. J. of Comp. Vision* 12, 1 (Jan.), 79–104.
- GUÉZIEC, A., PENNEC, X., AND AYACHE, N. 1997. Medical image registration using geometric hashing. *IEEE Computational Sci. Eng., Special Issue on Geometric Hashing* 4, 4, 29–41, Oct–Dec.
- GULLBERG, G. AND ZENG, G. 1992. A cone-beam filtered backpropagation reconstruction algorithm for cardiac single photon emission computed tomography. *IEEE Trans. on Med. Img.* MI-11, 91–101.
- GUO, D. AND RICHARDSON, P. 1998. Automatic vessel extraction from angiogram images. *IEEE Comput. Cardiol.* 25, 441–444.
- HARIS, K., EFSTRATIADIS, S. N., MAGLAVERAS, N., GOURASSAS, J., PAPPAS, C., AND LOURIDAS, G. 1997a. Automated coronary artey extraction using watersheds. *IEEE Comput. Cardiol.* 24, 741–744.
- HARIS, K., EFSTRATIADIS, S., MAGLAVERAS, N., AND PAPPAS, C. 1997b. Semi-automatic extraction of vascular networks in angiograms. In *IEEE Conf. Eng. in Medicine and Bio.* 1067–1068.
- HART, M. AND HOLLEY, L. 1993. A method of automated coronary artey tracking in unsubtracted angiograms. In *IEEE Comput. Cardiol.* 93–96.
- HART, W. E., GOLDBAUM, M., COTE, B., KUBE, P., AND NELSON, M. R. 1997. Automated measurement of retinal vascular tortuosity. In *Proc AMIA Fall Conference*.
- HAYKIN, S. 1994. *Neural Networks: A Comprehensive Foundation*. Mcmillan College, New York.
- HIGGINS, W., SPYRA, W., KARWOSKI, R., AND RITMAN, E. 1996. System for analyzing hig-resolution three-dimensional coronary angiograms. *IEEE Trans. on Med. Image* 15, 377–385.
- HIGGINS, W. E., SPYRA, W. J. T., RITMAN, E. L., KIM, Y., AND SPELMAN, F. A. 1989. Automatic extraction of the arterial tree from 3-d angiograms. In *IEEE Conf. Eng. in Medicine and Bio.* Vol. 2. 563–564.
- HOOVER, A., KOUZNETSOVA, V., AND GOLDBAUM, M. 2000. Locating blood vessels in retinal images by piecewise threshold probing of a matched filter response. *IEEE Trans. on Med. Image* 19, 3 (March), 203–210.
- HU, Y., ROGERS, W., COAST, D., KRAMER, C., AND REICHEK, N. 1998. Vessel boundary extraction based on a global and local deformable physical model with variable stiffness. *Magne. Reson. Imaging* 16, 8, 943–951.
- HUANG, Q. AND STOCKMAN, G. 1993. Generalized tube model: Recognizing 3d elongated objects from 2d intensity images. In *Proc. of the IEEE Conf. on CVPR*. 104–109.

- HUNTER, I., SORAGHAN, J., AND McDONAGH, T. 1995. Fully automatic left ventricular boundary extraction in echocardiographic images. In *IEEE Computers in Cardiology*. 741–744.
- JAIN, R., KASTURI, R., AND SCHUNCK, B. 1995. *Machine Vision*. McGH.
- KALITZIN, S., TER HAAR ROMANEY, B., SALDEN, A., NACKEN, P., AND VIERGEVER, M. 1998. Topological numbers and singularities in scalar images: Scale-space evolution properties. *J. Math. Imaging and Vis.* 9, 253–269.
- KASS, M., WITKIN, A., AND TERZOPOULOS, D. 1988. Snakes: Active contour models. *Int. J. Comput. Vision* 1, 4, 321–331.
- KAWATA, Y., NIKI, N., AND KUMAZAKI, T. 1995a. An approach for detecting blood vessel diseases from cone-beam CT image. In *IEEE Int. Conf. on Image Processing*. 500–503.
- KAWATA, Y., NIKI, N., KUMAZAKI, T., AND MOONIER, P. 1995b. Characteristics measurement for blood vessel diseases detection based on cone-beam ct images. In *IEEE Nuclear Science Symposium and Medical Imaging Conference*. Vol. 3. 1660–1664.
- KAYIKCIOGLU, T. AND MITRA, S. 1992. Unique determination of shape and area of coronary arterial cross-section from biplane angiograms. In *IEEE Comp.-Based Med. Sys.* 596–603.
- KAYIKCIOGLU, T. AND MITRA, S. 1993. A new method for estimating dimensions and 3-d reconstruction of coronary arterial trees from biplane angiograms. In *IEEE Comp.-Based Med. Sys.* 153–158.
- KIRBAS, C. AND QUEK, F. 2002. 3d wave propagation and traceback in vascular extraction. In *IEEE Eng. in Medicine and Bio. and Biomed. Eng. Soc.*
- KITAMURA, K., TOBIS, J., AND SKLANSKY, J. 1988a. Biplane analysis of atherosomatous coronary arteries. In *Proc. Int. Conf. Pattern Rec.* Vol. 2. 1277–1281.
- KITAMURA, K., TOBIS, J., AND SKLANSKY, J. 1988b. Estimating the 3-d skeletons and transverse areas of coronary arteries from biplane angiograms. *IEEE Trans. on Med. Img.* 7, 173–187.
- KLEIN, A., EGGLIN, T., POLLAK, J., LEE, F., AND AMINI, A. 1994. Identifying vascular features with orientation specific filters and b-spline snakes. In *IEEE Computers in Cardiology*. 113–116.
- KLEIN, A., LEE, F., AND AMINI, A. 1997. Quantitative coronary angiography with deformable spline models. *IEEE Trans. on Med. Img.* 16, 468–482.
- KOENDERINK, J. 1990. *Solid shapes*. MITP.
- KOHONEN, T. 1995. *Self-organizing Maps*. Springer-Verlag, New York.
- KOLLER, T. M., GERIG, G., SZÉKELY, G., AND DETTWILER, D. 1995. Multiscale detection of curvilinear structures in 2d and 3d image data. In *Int. Conf. on Comp. Vision*. 864–869.
- KOMPATSIARIS, I., TZOVARAS, D., KOUTKIAS, V., AND STRINTZIS, M. 2000. Deformable boundary detection of stents in angiographic images. *IEEE Trans. on Med. Img.* 19, 6 (June), 652–662.
- KOTTKE, D. AND SUN, Y. 1990a. Region splitting of medical images based upon bimodality analysis. In *IEEE Eng. Conf. in Medicine and Bio.* Vol. 12. 154–155.
- KOTTKE, D. AND SUN, Y. 1990b. Segmentation of coronary arteriograms by iterative ternary classification. *IEEE Trans. on Biomed. Engr.* 37, 778–785.
- KOZERKE, S., BOTNAR, R., OYRE, S., SCHEIDECKER, M. B., PEDERSEN, E., AND BOESINGER, P. 1999. Automatic vessel segmentation using active contours in cine phase contrast flow measurements. *J. of Mag. Res. Imaging* 10, 1 (July), 41–51.
- KRISSIAN, K., MALANDAIN, G., AND AYACHE, N. 1996. Directional anisotropic diffusion applied to segmentation of vessels in 3d images. Tech. Rep. 3064, INRIA.
- KRISSIAN, K., MALANDAIN, G., AND AYACHE, N. 1998. Model-based multiscale detection and reconstruction of 3d vessels. Tech. Rep. 3442, INRIA.
- KRISSIAN, K., MALANDAIN, G., AYACHE, N., VAILLANT, R., AND TROUSSET, Y. 1998a. Model-based multiscale detection of 3d vessels. *Proc. of the IEEE Conf. on CVPR*, 722–727.
- KRISSIAN, K., MALANDAIN, G., AYACHE, N., VAILLANT, R., AND TROUSSET, Y. 1998b. Model-based multiscale detection of 3d vessels. In *Proc. IEEE Workshop Biomed. Image Anal.* 202–208.
- KRISSIAN, K., MALANDAIN, G., AYACHE, N., VAILLANT, R., AND TROUSSET, Y. 1999. Model based detection of tubular structures in 3d images. Tech. Rep. 3736, INRIA.
- LECORNU, L., ROUX, C., AND JACQ, J. 1994. Extraction of vessel contours in angiograms by simultaneous tracking of the two edges. In *IEEE Conf. Eng. in Medicine and Bio.* Vol. 1. 678–679.
- LINDEBERG, T. 1994. *Scale-Space theory in Computer Vision*. Kluwer Academic Publishers, Dordrecht, Netherlands.
- LINDEBERG, T. 1996. Edge detection and ridge detection with automatic scale selection. In *Proc. of the IEEE Conf. on CVPR*. 465.
- LIU, I. AND SUN, Y. 1993. Recursive tracking of vascular networks in angiograms based on the detection-deletion scheme. *IEEE Trans. on Med. Img.* 12, 334–341.
- LORENZ, C., CARSE, I. C., BUZUG, T. M., FASSNACHT, C., AND WEESE, J. 1997. Multi-scale line segmentation with automatic estimation of width, contrast and tangential direction in 2d and 3d medical images. In *Joint Conf. Comp. Vision, Vir. Reality and Robotics in Medicine and Robotics, and Comput. Assisted Surgery*. 213–222.
- LU, S. AND EIHO, S. 1993. Automatic detection of the coronary arterial contours with sub-branches from an x-ray angiogram. In *IEEE Computers in Cardiology*. 575–578.

- LUO, H., QIANG, L., ACHARYA, R., AND GABORSKI, R. 2000. Robust snake model. In *Proc. IEEE Conf. on CVPR*. Vol. 1. 452–457.
- MALLADI, R., SETHIAN, J. A., AND VEMURI, B. C. 1995. Shape modeling with front propagation: A level set approach. *PAMI* 17, 2 (Feb.), 158–175.
- MAO, F., RUAN, S., BRUNO, A., TOUMOULIN, C., COLLOREC, R., AND HAIGRON, P. 1992. Extraction of structural features in digital subtraction angiography. In *IEEE Int. Biomed. Eng. Days*. 166–169.
- MARTELLI, A. 1976. An application of heuristic search methods to edge and contour detection. In *Commun. ACM* 19, 73–83.
- MAYER, H., LAPTEV, I., BAUMGARTNER, A., AND STEGER, C. 1997. Automatic road extraction based on multi-scale modeling, context, and snakes. *IEEE Trans. on Med. Image* 32, 47–56.
- MCINERNEY, T. AND TERZOPoulos, D. 1995. Topologically adaptable snakes. In *Int. Conf. on Comp. Vision*. 840–845.
- MCINERNEY, T. AND TERZOPoulos, D. 1996. Deformable models in medical image analysis: A survey. *IEEE Medical Image Analysis* 1, 2, 91–108.
- MCINERNEY, T. AND TERZOPoulos, D. 1997. Medical image segmentation using topologically adaptable surfaces. In *Conf. Comp. Vision, Vir. Reality and Robotics in Medicine and Robotics*. Vol. 1205. 23–32.
- MILLER, J., BREEN, D., LORENSEN, W., O'BARA, R., AND WOZNY, M. 1991. Geometrically deformed models: A method for extracting closed geometric models from volume data. *CG* 25, 4 (July), 217–226.
- MOLINA, C., PRAUSE, G., RADEVA, P., AND SONKA, M. 1998. 3-d catheter path reconstruction from biplane angiograms. In *SPIE*. Vol. 3338. 504–512.
- MONGA, O., ARMANDE, N., AND MONTESINOS, P. 1997. Thin nets and crest lines: Application to satellite data and medical images. *Computer Vision and Image Understanding* 66, 1.
- MONGA, O., LENGAGNE, R., AND DERICHE, R. 1994a. Crest-lines extraction in volumetric 3d medical images: a multiscale approach. In *Proc. Int. Conf. Pattern Rec.*
- MONGA, O., LENGAGNE, R., AND DERICHE, R. 1994b. Extraction of the zero-crossings of the curvature derivatives in volumic 3d medical images: A multi-scale approach. In *Proc. of the IEEE Conf. on CVPR*. 852–855.
- NEKOVEI, R. AND SUN, Y. 1995. Back-propagation network and its configuration for blood vessel detection in angiograms. *IEEE Trans. on Neural Nets* 6, 1 (January), 64–72.
- NGUYEN, T. AND SKLANSKY, J. 1986a. Computing the skeleton of coronary arteries in cineangiograms. *Comput. and Biomed. Res.* 19, 428–444.
- NGUYEN, T. AND SKLANSKY, J. 1986b. A fast skeleton finder for coronary arteries. In *Proc. Int. Conf. Pattern Rec.* 481–483.
- NIKI, N., KAWATA, Y., SATO, H., AND KUMAZAKI, T. 1993. 3d imaging of blood vessels using x-ray rotational angiographic system. *IEEE Med. Imaging Conf.* 3, 1873–1877.
- O'BRIEN, J. F. AND EZQUERRA, N. F. 1994. Automated segmentation of coronary vessels in angiographic image sequences utilizing temporal, spatial structural constraints. In *Proc. SPIE Conf. Visualization in Biomed. Computing*.
- O'DONNELL, T., BOULT, T. E., FANG, X., AND GUPTA, A. 1994. The extruded generalized cylinder: A deformable model for object recovery. In *Proc. of the IEEE Conf. on CVPR*. 174–181.
- O'DONNELL, T., GUPTA, A., AND BOULT, T. 1997. A new model for the recovery of cylindrical structures from medical image data. In *Joint Conf. Comp. Vision, Vir. Reality and Robotics in Medicine and Robotics, and Comp.-Assisted Surgery*. 223–232.
- OSHER, S. AND SETHIAN, J. A. 1988. Fronts propagating with curvature dependent speed: Algorithms based on hamilton-jacobi formulation. *J. Computat. Phys.* 79, 12–49.
- OTSU, N. 1979. A threshold selection method from gray-level histograms. *IEEE Trans. on Syst., Man, and Cybernet.* 9, 62–66.
- PARK, S., LEE, J., KOO, J., KWON, O., AND HONG, S. 1997. Adaptive tracking algorithm based on direction field using ml estimation in angiogram. In *IEEE Conference on Speech and Image Technologies for Computing and Telecommunications*. Vol. 2. 671–675.
- PARKER, D. L., WU, J., AND VAN BREE, R. E. 1988. Three dimensional vascular reconstruction from projections: A theoretical review. In *IEEE Conf. Eng. in Medicine and Bio.*
- PARVIN, B. A., PENF, C., JOHNSTON, W., AND MAESTRE, F. M. 1994. Tracking of tubular objects for scientific applications. In *Proc. of the IEEE Conf. on CVPR*. 295–301.
- PELLOT, C., HERMENT, A., AND SIGELLE, M. 1994. A 3d reconstruction of vascular structures from two x-ray angiograms using an adapted simulated annealing algorithm. *IEEE Trans. on Med. Img.* 13, 48–60.
- PERONA, P. AND MALIK, J. 1990. Scale-space and edge detection using anisotropic diffusion. *PAMI* 12, 7 (July), 629–639.
- PETROCELLI, R., ELION, J., AND MANBECK, K. M. 1992. A new method for structure recognition in unsubtracted digital angiograms. In *IEEE Computers in Cardiology*. 207–210.
- PETROCELLI, R., MANBECK, K., AND ELION, J. 1993. Three dimensional structure recognition in digital angiograms using gauss-markov methods. In *IEEE Computers in Cardiology*. 101–104.
- PHAM, D., XU, C., AND PRINCE, J. 2000. *Current Methods in Medical Image Segmentation*. Vol. 2. 315–338.

- PITAS, I. AND VENETSANOPoulos, A. 1990. *Nonlinear Digital Filters: principles and applications*. Kluver Academic, Norwell, Mass.
- PIZER, S., MORSE, B., AND FRITSCH, D. 1998. Zoom-invariant vision of figural shape: the mathematics of cores. *Computer Vision and Image Understanding* 69, 55–71.
- POLI, R. AND VALLI, G. 1997. An algorithm for real-time vessel enhancement and detection. *Comp. Methods and Prog. in Biomed.* 52, 1 (Jan.), 1–22.
- PRINET, V., MONGA, O., GE, C., XIE, S., AND MA, S. 1996. Thin network extraction in 3d images: Application to medical angiograms. In *Proc. Int. Conf. Pattern Rec.* 386–390.
- PRINET, V., MONGA, O., AND ROCCHISANI, J. 1997. Multi-dimensional vessel extraction using crest lines. In *IEEE Conf. Eng. in Medicine and Bio.* Vol. 1. 393–394.
- PUIG, P. 1998a. Cerebral blood vessels modeling. Tech. Rep. LSI-98-21-R, PICS.
- PUIG, P. 1998b. Discrete medial axis transform for discrete objects. Tech. Rep. LSI-98-20-R, PICS.
- QUEK, F. AND KIRBAS, C. 2001. Vessel extraction in medical images by wave propagation and traceback. *IEEE Trans. on Med. Img.* 20, 2 (Feb.), 117–131.
- QUEK, F., KIRBAS, C., AND CHARBEL, F. 1999. Aim:attentionally-based interaction model for the interpretation of vascular angiograph. *IEEE Trans. on Inf. Tech. in Biomed.* 3, 2 (June), 139–150.
- QUEK, F., KIRBAS, C., AND CHARBEL, F. 2001. Aim: An attentionally-based system for the interpretation of angiography. In *Proc. IEEE Med. Imaging and Augmented Reality Conf.* 168–173.
- QUEK, F., KIRBAS, C., AND GONG, X. 2001. Simulated wave propagation and traceback in vascular extraction. In *Proc. IEEE Med. Imaging and Augmented Reality Conf.* 229–234.
- RIPLEY, B. 1996. *Pattern Recognition and Neural Networks*. Cambridge University Press.
- RITCHINGS, R. AND COLCHESTER, A. 1986. Detection of abnormalities on carotid angiograms. *Pattern Rec. Lett.* 4, 367–374.
- ROSENFIELD, A. AND SMITH, R. 1981. Thresholding using relaxation. *PAMI* 3, 598–606.
- ROST, U., MUNKEL, H., AND LIEDTKE, C.-E. 1998. A knowledge based system for the configuration of image processing algorithms. *Fachtagung Informations und Mikrosystem Technik*.
- RUECKERT, D. AND BURGER, P. 1995. Contour fitting using stochastic and probabilistic relaxation for cine mr images. In *Computer Assisted Radiology*. 137–142.
- RUECKERT, D. AND BURGER, P. 1996. Shape-based tracking and analysis of the aorta in cardiac mr images using geometrically deformable templates. In *Computer Assisted Radiology*.
- RUECKERT, D., BURGER, P., FORBAT, S. M., MOHIADDIN, R. D., AND YANG, G. Z. 1997. Automatic tracking of the aorta in cardiovascular mr images using deformable models. *IEEE Trans. on Med. Img.* 16, 5 (Oct.), 581–590.
- SARRY, L. AND BOIRE, J. 2001. Three-dimensional tracking of coronary arteries from biplane angiographic sequences using parametrically deformable moodels. *IEEE Trans. on Med. Img.* 20, 12 (Dec.), 1341–1351.
- SARWAL, A. AND DHAWAN, A. 1994. 3-d reconstruction of coronary arteries. In *IEEE Conf. Eng. in Medicine and Bio.* Vol. 1. 504–505.
- SATO, Y., ARAKI, T., HANAYAMA, M., NAITO, H., AND TAMURA, S. 1998a. A viewpoint determination system for stenosis diagnosis and quantification in coronary angiographic image acquisition. *IEEE Trans. on Med. Img.* 17, 121–137.
- SATO, Y., NAKAJIMA, S., SHIRAGA, N., ATSUMI, H., YOSHIDA, S., KOLLER, T., GERIG, G., AND KIKINIS, R. 1998b. 3d multi-scale line filter for segmentation and visualization of curvilinear structures in medical images. *IEEE Medical Image Analysis* 2, 2 (June), 143–168.
- SCHMITT, H., GRASS, M., RASCHE, V., SCHRAMM, O., HAENNEL, S., AND SARTOR, K. 2002. An x-ray-based method for the determination of the contrast agent propagation in 3-d vessel structures. *IEEE Trans. on Med. Img.* 21, 3 (Mar.), 251–262.
- SETHIAN, J. 1999. *Level Set Methods and Fast Marching Methods:Evolving Interfaces in Computational Geometry, Fluid Mechanics, Computer Vision, and Material Science*. Cambridge University Press, Cambridge, UK.
- SETHIAN, J. A. 1996. A fast marching level set method for monotonically advancing fronts. In *Proc. of Nat. Acad. of Sci.* Vol. 93. 1591–1595.
- SHEN, H. AND JOHNSON, C. R. 1994. Semi-automatic image segmentation: A bimodal thresholding approach. Tech. Rep. UUCS-94-019, Univ. of Utah, Dept. of Comput. Science.
- SHIFFMAN, S., RUBIN, G. D., AND NAPEL, S. 1996. *Semiautomated Editing of Computed Tomography Sections for Visualization of Vasculature*. Vol. 2707. SPIE.
- SMETS, C., VERBEECK, G., SUETENS, P., AND OOSTERLINCK, A. 1988. A knowledge-based system for the delineation of blood vessels on subtraction angiograms. *Pattern Rec. Lett.* 8, 113–121.
- SONKA, M., HLAVAC, V., AND BOYLE, R. 1999. *Image Processing, Analysis, and Machine Vision*. PWS Publishing.
- SORANTIN, E., HALMAI, C., ERDOHELYI, B., PALAGYI, K., NYUL, L., OLLE, K., GEIGER, B., LINDBICHLER, F., FRIEDRICH, G., AND KIESLER, K. 2002. Spiral-ct-based assessment of tracheal stenoses using 3-d-skeletonization. *IEEE Trans. on Med. Img.* 21, 3 (Mar.), 263–273.
- STANSFIELD, S. 1986. Angy: A rule-based expert system for automatic segmentation of coronary vessels from digital subtracted angiograms. *PAMI* 8, 3 (Mar.), 188–199.

- STEVENSON, D. 1987. Working towards the automatic detection of blood vessels in x-ray angiograms. *Pattern Rec. Lett.* 6, 107–112.
- STOCKETT, M. AND SOROKA, B. 1992. Extracting spinal cord contours from transaxial mr images using computer vision techniques. In *IEEE Comp.-Based Med. Sys.* 1–8.
- SUMMERS, P. AND BHALERAO, A. 1995. Derivation of pressure gradients from magnetic resonance angiography using multi-resolution segmentation. In *Proceedings of International Conference on Image Processing and its Applications*. 404–408.
- SUN, Y. 1989. Automated identification of vessel contours in coronary arteriograms by an adaptive tracking algorithm. *IEEE Trans. on Med. Img.* 8, 78–88.
- THACKRAY, B. AND NELSON, A. 1993. Semi-automatic segmentation of vascular network images using a rotating structuring element (rose) with mathematical morphology and dual feature thresholding. *IEEE Trans. on Med. Img.* 12, 385–392.
- THIRION, B., BASCLE, B., RAMESH, V., AND NAVAB, N. 2000. Fusion of color, shading and boundary information for factory pipe segmentation. In *Proc. of the IEEE Conf. on CVPR*. Vol. 2. 349–356.
- TOLEDO, R., ORRIOLS, X., BINEFA, X., RAVEDA, P., VITRIA, J., AND VILLANUEVA, J. J. 2000. Tracking elongated structures using statistical snakes. In *Proc. of the IEEE Conf. on CVPR*. 157–162.
- TOLIAS, Y. AND PANAS, S. 1998. A fuzzy vessel tracking algorithm for retinal images based on fuzzy clustering. *IEEE Trans. on Med. Img.* 17, 263–273.
- TOZAKI, T., KAWATA, Y., NIKI, N., OHMATSU, H., AND MORIYAMA, N. 1995. 3-d visualization of blood vessels and tumor using thin slice ct. In *IEEE Nuclear Science Symposium and Medical Imaging Conference*. Vol. 3. 1470–1474.
- UMBAUGH, S. 1998. *Computer Vision and Machine Processing*. PHPTR.
- VAN DER WEIDE, R., BAKKER, C., AND VIERGEVER, M. 2001. Localization of intravascular devices with paramagnetic markers in mr images. *IEEE Trans. on Med. Img.* 20, 10 (October), 1061–1071.
- WOOD, S., QU, G., AND ROLOFF, L. 1995. Detection and labeling of retinal vessels for longitudinal studies. In *IEEE Int. Conf. on Image Processing*. Vol. 3. 164–167.
- XU, C., PHAM, D., AND PRINCE, J. 2000. *Medical Image Segmentation Using Deformable Models*. SPIE Press, Chapter 3, 129–174.
- XU, C. AND PRINCE, J. 1998. Snakes, shapes, and gradient vector flow. *IEEE Trans. on Image Proces.* 7, 359–369.
- YIM, P., CHOYKE, P., AND SUMMERS, R. 2000. Gray-scale skeletonization of small vessels in magnetic resonance angiography. *IEEE Trans. on Med. Img.* 19, 6 (June), 568–576.
- ZANA, F. AND KLEIN, J. 1997. Robust segmentation of vessels from retinal angiography. In *IEEE International Conference on Digital Signal Processing*. Vol. 2. 1087–1090.
- ZERROUG, M. AND NEVATIA, R. 1993. Quasi-invariant properties and 3-d shape recovery of non-constant generalized cylinders. In *Proc. of the IEEE Conf. on CVPR*. 96–103.
- ZHOU, L., RZESZOTARSKI, M., SINGERMAN, L., AND CHOKREFF, J. 1994. The detection and quantification of retinopathy using digital angiograms. *IEEE Trans. on Med. Img.* 13, 619–626.

Received February 2003; accepted July 2004